
Graph Your Own Prompt

Xi Ding^{1,3}, Lei Wang^{1,2,†}, Piotr Koniusz^{2,3,4}, Yongsheng Gao^{1,†}
¹Griffith University, ²Data61/CSIRO,
³Australian National University, ⁴University of New South Wales

Abstract

We propose Graph Consistency Regularization (GCR), a novel framework that injects relational graph structures, derived from model predictions, into the learning process to promote class-aware, semantically meaningful feature representations. Functioning as a form of *self-prompting*, GCR enables the model to refine its internal structure using its own outputs. While deep networks learn rich representations, these often capture noisy inter-class similarities that contradict the model’s predicted semantics. GCR addresses this issue by introducing parameter-free *Graph Consistency Layers* (GCLs) at arbitrary depths. Each GCL builds a batch-level feature similarity graph and aligns it with a global, class-aware masked prediction graph, derived by modulating softmax prediction similarities with intra-class indicators. This alignment enforces that feature-level relationships reflect class-consistent prediction behavior, acting as a *semantic regularizer* throughout the network. Unlike prior work, GCR introduces a multi-layer, cross-space graph alignment mechanism with adaptive weighting, where layer importance is learned from graph discrepancy magnitudes. This allows the model to prioritize semantically reliable layers and suppress noisy ones, enhancing feature quality without modifying the architecture or training procedure. GCR is model-agnostic, lightweight, and improves semantic structure across various networks and datasets. Experiments show that GCR promotes cleaner feature structure, stronger intra-class cohesion, and improved generalization, offering a new perspective on learning from prediction structure. [\[Project website\]](#) [\[Code\]](#)

1 Introduction

Deep neural networks have achieved impressive success across a wide range of classification tasks, from natural images to medical diagnostics and scene understanding [88, 117, 111, 23, 26, 27, 28]. A key factor underlying this success is the ability of deep models to learn rich internal representations. However, despite their effectiveness, these representations are often noisy, entangled, and lack clear alignment with semantic class boundaries. This discrepancy can lead to feature spaces where samples from different classes remain closely aligned, undermining generalization and limiting the interpretability and robustness of learned models.

Intuitively, if a network is confident that two inputs belong to the same class, as indicated by their softmax predictions, then their intermediate representations should also reflect this similarity. Conversely, samples predicted to belong to different classes should ideally be separated in feature space. Yet, existing architectures and loss functions typically do not enforce such consistency between feature- and prediction-level relationships [90, 106, 108]. While contrastive learning and graph-based regularizers have emerged to structure feature spaces, they often require explicit positive/negative sampling or operate at a single level of abstraction, leaving much of the internal network dynamics unregulated [105, 64, 81].

[†] Corresponding authors: l.wang4@griffith.edu.au, yongsheng.gao@griffith.edu.au

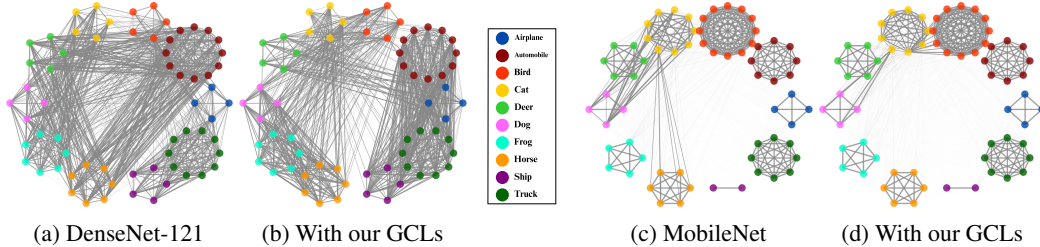


Figure 1: Relational graph visualization using a batch of 64 samples from CIFAR-10 on (left) DenseNet-121 and (right) MobileNet. We compare the baselines with their counterparts augmented by our GCLs. Our method promotes richer, class-aware semantic representations by acting as a form of *self-prompting*. For DenseNet-121, the baseline feature relational graph tends to connect samples based on superficial visual similarity (e.g., deer, horse, and automobile), often ignoring semantic boundaries. In contrast, our GCL-enhanced model produces more *semantically coherent groupings*, clearly separating animals from vehicles. On MobileNet, the prediction relational graph further highlights the strength of our method, demonstrating cleaner, more distinct class relationships compared to the baseline. These improvements reflect the effectiveness of our model in aligning feature and prediction spaces with semantic structure, despite being *lightweight and parameter-free*.

In this work, we propose a new form of structural supervision that enforces relational graph consistency between features and predictions throughout the network. We introduce Graph Consistency Regularization (GCR), a lightweight and general-purpose method that inserts Graph Consistency Layers (GCLs) after arbitrary network blocks/layers. Each GCL builds a batch-level feature relational graph using pairwise relations. These feature graphs are aligned with a class-aware masked prediction graph that encodes semantic similarity based on softmax outputs and label-derived intra-class indicators. The core idea is to treat the prediction graph as a reference structure, and guide the network to shape its internal feature geometry to be consistent with semantically meaningful predictions.

GCR is architecture-agnostic, lightweight, and introduces no new parameters. Importantly, it provides multi-layer supervision by aligning feature-prediction structures at multiple depths, using dynamically learned layer-wise weights. This acts as a regularization signal that sharpens class boundaries, suppresses noisy inter-class affinities, and encourages feature representations that reflect class semantics more faithfully (Fig. 1 provides a comparison). Our **contributions** are summarized as follows:

- i. We are the first to use dynamic, batch-level relational graphs to guide the learning process using class-aware prediction structures, enabling a new form of semantic regularization.
- ii. We introduce Graph Consistency Layers (GCLs), lightweight, parameter-free modules that can be flexibly inserted into existing networks, enabling multi-scale structural supervision with adaptively learned layer-wise weighting based on graph discrepancy.
- iii. We propose Graph Consistency Regularization (GCR), a novel framework that enforces alignment between intermediate feature graphs and global, class-aware prediction graphs, promoting semantic coherence and representation consistency throughout the network.

We validate GCR across diverse architectures and benchmarks, achieving consistent accuracy gains and stronger generalization without altering backbone design or training protocol. Below, we review related work.

2 Related Work

Graph-based representation learning. Graph-based methods [54, 16] have been widely adopted to model relationships among samples, particularly in non-Euclidean domains such as social networks or molecules [1, 53, 121]. In classification tasks, graphs have been used to capture instance-level similarities for label propagation [113, 74], semi-supervised learning [115, 114], and contrastive representation learning [20, 91]. For example, some methods build graphs over entire datasets [101] or memory banks [9, 3] to encourage feature consistency via graph Laplacian regularization [80, 4] or message passing [38, 79]. Unlike these approaches, which require maintaining global graphs or rely

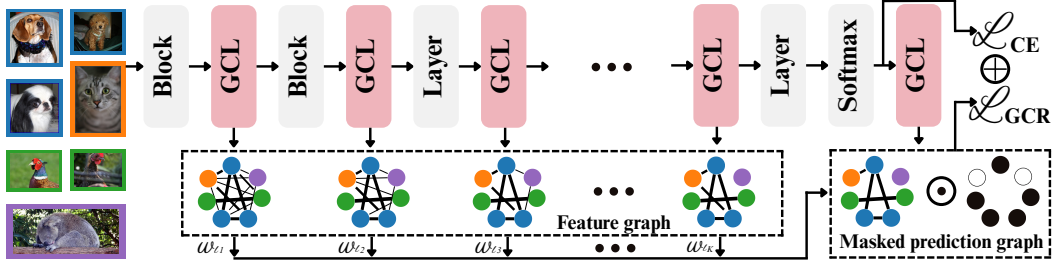


Figure 2: Our *parameter-free* Graph Consistency Layer (GCL), highlighted in red, can be inserted after any micro-network block (*e.g.*, Inception) or specific layer (*e.g.*, fully connected). Each GCL constructs a relational graph from batch-level features using a similarity metric (*e.g.*, cosine). A reference graph is generated from softmax predictions and masked by intra-class indicators: binary masks identifying semantically consistent pairs. Each GCL enforces alignment between masked prediction graph and the feature-level graphs. The resulting consistency signals are adaptively weighted, forming the Graph Consistency Regularization (GCR) framework, which integrates with the primary loss (*e.g.*, cross-entropy), acting as a *semantic regularizer* to guide learning.

on graph neural networks (GNNs), our method operates locally within each batch and uses graphs constructed dynamically from features and predictions, avoiding architectural overhead.

Contrastive and metric learning. Contrastive learning has emerged as a powerful framework for self-supervised and supervised representation learning [110, 69, 60]. These methods typically pull together positive pairs (*e.g.*, same-class or augmented views) and push apart negatives. Extensions such as supervised contrastive learning and hard negative mining improve class discrimination by incorporating label information [66, 105]. However, these approaches often rely on explicit sampling strategies or carefully tuned augmentations, and are usually applied at a single point in the network. In contrast, our method requires no sampling, no data augmentation, and aligns structural relationships across multiple network depths, offering a form of contrast without contrastive pairs.

Regularization and feature structure learning. Various regularization techniques aim to improve generalization by shaping the geometry of learned feature spaces [57, 78]. For instance, center loss [86, 84] and triplet loss [24, 119, 29] enforce compactness or margin between classes. Other works apply orthogonality or decorrelation constraints on activations or weights [71, 104]. More recently, structural regularizers use pairwise distances or affinity matrices to inject relational constraints into training [73, 59]. Compared to these, our approach enforces cross-space structural alignment, between features and softmax-based predictions, while incorporating class-aware masking to focus only on semantically meaningful relationships.

Layer-wise supervision and structural alignment. Supervision at intermediate layers has shown promise in improving training dynamics and interpretability [52, 126, 39]. Auxiliary losses [93, 43], attention distillation [2, 50, 75], and intermediate contrastive losses [103, 15, 86] are examples where internal representations are guided explicitly. However, these methods typically supervise layers independently, and rarely use the structural information from model outputs to regularize feature learning [18, 100, 122, 129]. Our approach introduces a new form of semantic structure supervision by aligning feature similarity graphs with a masked prediction graph across multiple layers, with learnable or depth-based weighting to adaptively emphasize useful features during training.

A discussion of GCR’s relationship to existing paradigms is presented in Appendices A and B. Below, we present our proposed method.

3 Method

We introduce the Graph Consistency Layer (GCL), a lightweight module that can be inserted at any layer or micro-architecture block (*e.g.*, a convolutional layer or an inception block, see Fig. 2). Each GCL dynamically constructs a relational graph from intermediate features and aligns it with a semantic graph derived from the model’s own predictions within each training batch. This alignment is driven by Graph Consistency Regularization (GCR), a novel technique that promotes semantically coherent and geometrically structured feature learning. Our motivation is discussed in Appendix C.

3.1 Graph Consistency Layer

Relational graph construction on features. Given a batch of feature activations at layer l , represented by the feature matrix $\mathbf{X}^{(l)} \in \mathbb{R}^{n \times d}$ (where we vectorize or flatten high-dimensional feature maps), with n being the batch size and d the feature dimension, we construct a pairwise relational graph $\mathbf{F}^{(l)} \in \mathbb{R}^{n \times n}$ that encodes the relationships between features within the batch. For simplicity, we use cosine similarity to compute the relationship between the i -th and j -th samples as follows:

$$\mathbf{F}_{ij}^{(l)} = \text{ReLU} \left(\cos(\mathbf{x}_i^{(l)}, \mathbf{x}_j^{(l)}) \right) \quad (1)$$

This formulation captures local geometric relationships in feature space. However, the raw feature graph $\mathbf{F}^{(l)} \in \mathbb{R}^{n \times n}$ may contain spurious correlations that misalign with true semantic class boundaries. To address this, a semantic reference graph is introduced to guide feature alignment.

Masked relational graph on predictions. To construct the reference graph, we use the network’s prediction logits $\mathbf{Z} \in \mathbb{R}^{n \times C}$, where C is the number of classes and \mathbf{Z} contains the pre-softmax output scores. From these logits, we compute class probabilities via the softmax function, and then calculate the pairwise similarity between prediction vectors $\mathbf{z}_i, \mathbf{z}_j \in \mathbb{R}^C$ of the i -th and j -th samples as:

$$\mathbf{S}_{ij} = \text{ReLU} \left(\cos(\text{softmax}(\mathbf{z}_i), \text{softmax}(\mathbf{z}_j)) \right). \quad (2)$$

The resulting matrix $\mathbf{S} \in \mathbb{R}^{n \times n}$ captures the pairwise similarities between the predicted class distributions of samples. However, not all prediction similarities are equally informative for guiding feature alignment, particularly (i) in the early stages of training, when predictions are often noisy and lack well-formed class semantics, and (ii) in cases where inherently ambiguous or visually similar classes introduce misleading affinities. To focus on semantically consistent pairs, we introduce a binary mask $\mathbf{M} \in \{0, 1\}^{n \times n}$, where $\mathbf{M}_{ij} = 1$ if samples i and j share the same ground truth label, and 0 otherwise. The prediction relational graph \mathbf{P} is then defined as:

$$\mathbf{P}_{ij} = \mathbf{M}_{ij} \odot \mathbf{S}_{ij}, \quad (3)$$

where \odot denotes element-wise (Hadamard) multiplication. This graph retains only the prediction similarities between samples of the same class, effectively encoding intra-class semantic relationships while discarding noisy or misleading inter-class connections. Below, we outline our GCR framework.

3.2 Graph Consistency Regularization

Layer-wise graph alignment. GCR centers on aligning the feature graph $\mathbf{F}^{(l)}$ with the masked prediction graph \mathbf{P} . To encourage symmetric, undirected relationships and eliminate redundancy, we use only the strictly upper triangular part of the graphs, excluding the diagonal elements to remove self-connections. This design ensures that the graphs capture bidirectional affinities between samples without double-counting or emphasizing self-similarity. Such undirected structure often leads to more stable optimization and promotes balanced representation learning across the batch.

The graph alignment loss at layer l is defined as the squared Frobenius norm between the upper triangular parts of the two graphs:

$$\mathcal{L}_{\text{GCR}}^{(l)} = \|\text{triu}(\mathbf{F}^{(l)}) - \text{triu}(\mathbf{P})\|_F^2, \quad (4)$$

where $\text{triu}(\cdot)$ denotes the strictly upper triangular matrix. This loss compels the model to adjust intermediate features so their geometric structure aligns with the semantic topology encoded in the masked prediction relational graph.

Graph consistency aggregation. To enforce consistency across the network hierarchy, we aggregate alignment losses from a set of selected layers $\{1, \dots, K\}$. The total GCR loss is given by:

$$\mathcal{L}_{\text{GCR}} = \sum_{l \in \{1, \dots, K\}} w_l \cdot \|\text{triu}(\mathbf{F}^{(l)}) - \text{triu}(\mathbf{P})\|_F^2. \quad (5)$$

Here, w_l is a weight that balances the contribution of each layer. These weights can be either: (i) fixed, using depth-based heuristics such as equal ($w_l = 1/K$), linear ($w_l = l/K$), squared ($(l/K)^2$),

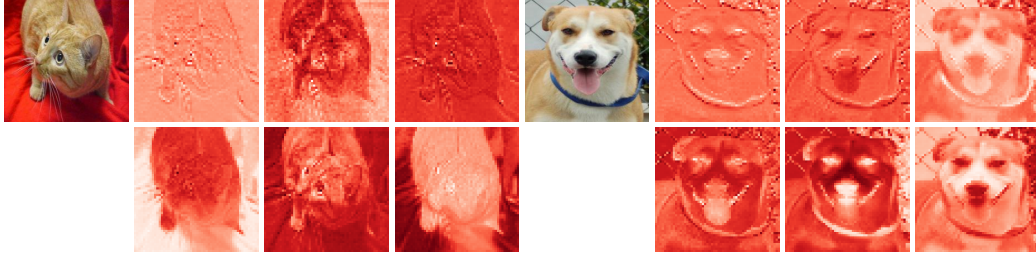


Figure 3: Feature map visualizations from models trained on *identical data batches*: (top) baseline and (bottom) our GCL-augmented model. Brighter red regions indicate stronger feature activations. Compared to the baseline, GCL-enhanced maps more clearly emphasize class-discriminative cues, e.g., cat faces, ears, and eyes, and for dogs, tongues, noses, and facial contours, reflecting improved focus and interpretability. GCL also yields higher classification accuracy (98.1% \rightarrow 99.8%).

square-root ($\sqrt{l/K}$), cosine ($\frac{1+\cos(\pi \frac{l}{K})}{2}$), or arccosine ($\frac{\arccos(1-2\frac{l}{K})}{\pi}$); or (ii) adaptive, based on current alignment quality:

$$w_l = \frac{\exp\left(-\|\text{triu}(\mathbf{F}^{(l)}) - \text{triu}(\mathbf{P})\|_F^2\right)}{\sum_{j=1}^K \exp\left(-\|\text{triu}(\mathbf{F}^{(j)}) - \text{triu}(\mathbf{P})\|_F^2\right)}. \quad (6)$$

The adaptive weighting ensures that layers with greater misalignment are given more importance during training, allowing the model to concentrate on refining representations that are less aligned with the desired semantic structure. We evaluate different weighting schemes in our experiments.

Training objective. The overall training loss is composed of two components: the standard cross-entropy loss, denoted as \mathcal{L}_{CE} , and the GCR loss, \mathcal{L}_{GCR} . The total loss function is given by:

$$\mathcal{L}_{\text{total}} = \mathcal{L}_{\text{CE}} + \lambda \cdot \mathcal{L}_{\text{GCR}}, \quad (7)$$

where λ is a hyperparameter that controls the relative contribution of the GCR term. A key advantage of GCR is that it introduces no additional parameters, and its graph alignment loss relies on matrix operations well-suited to modern hardware. Next, we present the theoretical foundations of GCR.

3.3 Theoretical Analysis of GCR

We present a theoretical analysis of GCR, linking its empirical design to core principles in statistical learning and spectral graph theory. Specifically, we show that minimizing the GCR loss: (i) reduces the effective hypothesis class capacity via covering number bounds[55, 123] and Dudley’s entropy integral[32]; (ii) promotes spectral alignment between learned features and semantic prediction graphs through normalized Laplacians[5]; and (iii) acts as a PAC-Bayesian regularizer[35], imposing a structural prior over the function space. Additional insights are provided in Appendix D.

Generalization via covering numbers. Let \mathcal{F}_L be the class of functions $f^{(l)} : \mathcal{X} \rightarrow \mathbb{R}^d$ representing layer- l embeddings. Assume the feature representations are uniformly bounded by a constant B in ℓ_2

norm: $\|f^{(l)}(x)\|_2 = \sqrt{\sum_{i=1}^d (f_i^{(l)}(x))^2} \leq B$, for all $x \in \mathcal{X}$. This is a standard constraint in learning theory to control hypothesis space capacity. In practice, with ℓ_2 normalization as used here, $B=1$. Next, we define a structurally-constrained hypothesis class:

$$\mathcal{F}_\epsilon := \left\{ f \in \mathcal{F}_L : \mathcal{L}_{\text{GCR}}^{(l)} := \|\text{triu}(\mathbf{F}^{(l)}) - \text{triu}(\mathbf{P})\|_F^2 \leq \epsilon \right\}, \quad (8)$$

which enforces alignment between feature and prediction graphs reflecting intra-class similarity.

Theorem 1 (Generalization via Dudley’s entropy integral). *Let $\ell(f(x), y)$ be a γ -Lipschitz loss function (e.g., cross-entropy), and let \mathcal{F}_L be the class of functions at layer l such that each function $f^{(l)}$ satisfies the ℓ_2 -bounded constraint $\|f^{(l)}(x)\|_2 \leq B$. Suppose $\mathcal{F}_\epsilon \subseteq \mathcal{F}_L$ is the subset of functions that are additionally constrained by the GCR alignment loss:*

$$\mathcal{L}_{\text{GCR}}^{(l)} = \frac{1}{n^2} \sum_{i,j=1}^n \left(\text{ReLU}(\langle \mathbf{x}_i^{(l)}, \mathbf{x}_j^{(l)} \rangle) - \mathbf{P}_{ij} \right)^2 \leq \epsilon, \quad (9)$$

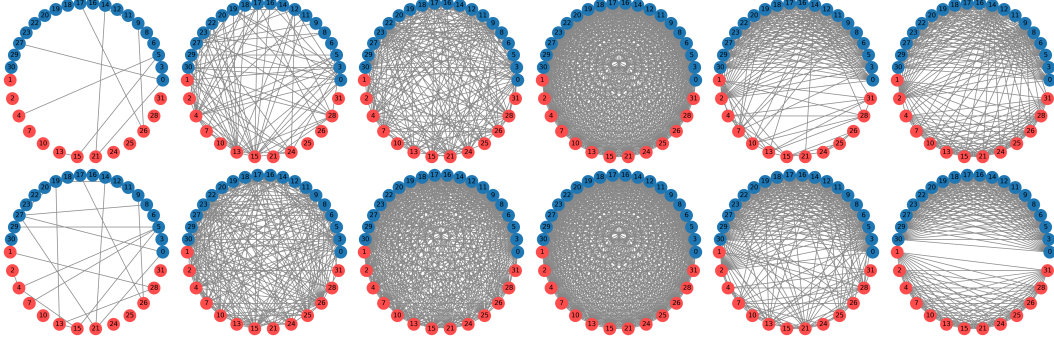


Figure 4: Relational graph visualization on Kaggle cats vs. dogs. We compare the best baseline model and our GCL-augmented model using the same batch of 32 samples (red = cat, blue = dog). The baseline consists of four convolutional blocks and two fully connected layers; our method inserts a Graph Consistency Layer (GCL) after each, totaling six GCLs. The top row shows the baseline (without GCLs); the bottom row shows our GCL-enhanced model. Each column visualizes the relational graph at a specific layer, from early features (left) to final predictions (right). Early layers exhibit weak connectivity, as low-level features poorly capture class semantics. As depth increases, both models shift toward more structured, class-separable relationships. GCLs amplify this effect by attenuating low-similarity inter-class edges and reinforcing intra-class coherence, leading to improved accuracy (98.1% vs. 99.8%). For clarity, edges with similarity < 0.4 are omitted.

where \mathbf{P}_{ij} is the target alignment between the normalized feature vectors $\mathbf{x}_i^{(l)}$ and $\mathbf{x}_j^{(l)}$. The GCR loss enforces that the angular distances between the feature vectors are small, meaning that the vectors are close to each other in the Euclidean space. If \mathcal{F}_ϵ admits a covering number bound:

$$\mathcal{N}(\mathcal{F}_\epsilon, \|\cdot\|_2, \alpha) \leq \left(\frac{C}{\alpha}\right)^d, \quad (10)$$

where $\mathcal{N}(\mathcal{F}_\epsilon, \|\cdot\|_2, \alpha)$ is the covering number of \mathcal{F}_ϵ with respect to the ℓ_2 norm, then the expected loss of a function $f \in \mathcal{F}_\epsilon$ is bounded with high probability by:

$$\mathbb{E}_{(x,y) \sim \mathcal{D}}[\ell(f(x), y)] \leq \frac{1}{n} \sum_{i=1}^n \ell(f(x_i), y_i) + \frac{12\gamma}{\sqrt{n}} \int_0^B \sqrt{d \log\left(\frac{C}{\alpha}\right)} d\alpha, \quad (11)$$

where $B = O(\sqrt{\epsilon})$ is the effective radius of function class \mathcal{F}_ϵ under the GCR constraint, and the second term represents the generalization error, which is controlled by the function class complexity.

Proof. The proof can be found in Appendix E. \square

Remark 1. This result shows that GCR reduces generalization error by shrinking the effective complexity of the function class. By aligning relational structure, GCR implicitly contracts the hypothesis space, leading to improved generalization.

Spectral alignment via normalized Laplacians. Let \mathbf{F} and \mathbf{P} be symmetric affinity matrices derived from feature embeddings and masked predictions, respectively. Their associated normalized graph Laplacians are defined as $\mathcal{L}_\mathbf{F} := \mathbf{I} - \mathbf{D}_\mathbf{F}^{-1/2} \mathbf{F} \mathbf{D}_\mathbf{F}^{-1/2}$ and $\mathcal{L}_\mathbf{P} := \mathbf{I} - \mathbf{D}_\mathbf{P}^{-1/2} \mathbf{P} \mathbf{D}_\mathbf{P}^{-1/2}$, where $\mathbf{D}_\mathbf{F}$ and $\mathbf{D}_\mathbf{P}$ are the degree matrices corresponding to \mathbf{F} and \mathbf{P} , i.e., $(\mathbf{D}_\mathbf{F})_{ii} = \sum_j \mathbf{F}_{ij}$ and similarly for $\mathbf{D}_\mathbf{P}$.

Proposition 1 (Spectral alignment). *Let \mathbf{F} and \mathbf{P} be symmetric matrices such that*

$$\|\mathbf{F} - \mathbf{P}\|_F \leq \epsilon, \quad \|\mathbf{D}_\mathbf{F} - \mathbf{D}_\mathbf{P}\| \leq \delta. \quad (12)$$

Then, there exists a constant $C > 0$ depending on spectral properties of the graphs (e.g., sparsity, minimum degree), such that

$$\|\mathcal{L}_\mathbf{F} - \mathcal{L}_\mathbf{P}\|_F \leq C(\epsilon + \delta). \quad (13)$$

Proof. The proof can be found in Appendix E. \square

Table 1: Accuracy (%) on CIFAR-10 across models. Results are shown for MobileNet (MNet), ShuffleNet (SN), SqueezeNet (SQNet), GoogLeNet (GLNet), ResNeXt-50/101 (Rx-50/101), ResNet-34/50/101 (R34/R50/R101), DenseNet-121 (D121), and MAE under various GCL configurations (Early, Mid, Late, combinations, Full). Bold indicates the best improvements over baselines; underlines mark the second-best. The final column shows the average accuracy for each configuration.

	MAE	MNet	SN	SQNet	GLNet	Rx-50	Rx-101	R34	R50	R101	D121	Mean
Baseline	88.95 \pm 0.33	90.23 \pm 0.25	91.21 \pm 0.28	92.30 \pm 0.25	94.10 \pm 0.26	94.57 \pm 0.29	95.12 \pm 0.30	94.83 \pm 0.25	95.03 \pm 0.28	95.22 \pm 0.31	95.01 \pm 0.27	93.32 \pm 2.26
Early GCL	89.42 \pm 0.25	91.17 \pm 0.22	92.33 \pm 0.33	92.59 \pm 0.21	94.89 \pm 0.23	95.48 \pm 0.22	95.63 \pm 0.25	95.55 \pm 0.18	95.57 \pm 0.23	95.39 \pm 0.26	95.81 \pm 0.17	93.98 \pm 2.22
Mid GCL	89.77 \pm 0.22	91.15 \pm 0.18	92.58 \pm 0.19	92.40 \pm 0.20	94.82 \pm 0.21	95.47 \pm 0.19	95.39 \pm 0.24	95.69 \pm 0.23	95.61 \pm 0.20	95.75 \pm 0.17	95.51 \pm 0.22	94.01 \pm 2.15
Late GCL	89.70 \pm 0.29	91.40 \pm 0.19	92.36 \pm 0.21	92.80 \pm 0.19	94.88 \pm 0.19	95.35 \pm 0.28	95.71 \pm 0.26	95.69 \pm 0.19	95.66 \pm 0.17	<u>95.51</u> \pm 0.24	<u>95.72</u> \pm 0.22	94.07 \pm 2.14
Early+Mid	89.52 \pm 0.19	90.77 \pm 0.26	92.56 \pm 0.21	92.27 \pm 0.25	94.79 \pm 0.18	95.33 \pm 0.27	95.55 \pm 0.23	95.46 \pm 0.20	95.51 \pm 0.21	95.37 \pm 0.19	95.64 \pm 0.20	93.89 \pm 2.22
Mid+Late	89.59 \pm 0.28	91.23 \pm 0.20	92.79 \pm 0.20	92.86 \pm 0.23	94.61 \pm 0.22	95.51 \pm 0.19	95.38 \pm 0.27	95.45 \pm 0.18	95.33 \pm 0.26	95.52 \pm 0.14	95.70 \pm 0.19	94.00 \pm 2.09
Early+Late	89.64 \pm 0.25	91.03 \pm 0.24	92.30 \pm 0.28	92.70 \pm 0.23	94.69 \pm 0.20	95.40 \pm 0.20	95.35 \pm 0.23	95.60 \pm 0.21	95.31 \pm 0.25	95.49 \pm 0.16	95.53 \pm 0.22	93.92 \pm 2.14
Full GCL	89.55 \pm 0.23	90.99 \pm 0.18	92.48 \pm 0.19	92.65 \pm 0.20	94.57 \pm 0.21	<u>95.50</u> \pm 0.19	95.34 \pm 0.20	95.48 \pm 0.17	<u>95.62</u> \pm 0.18	95.38 \pm 0.21	95.51 \pm 0.20	93.92 \pm 2.15

Corollary 1. *The GCR alignment loss, which encourages $\|\mathbf{F} - \mathbf{P}\|_F \leq \epsilon$, indirectly enforces spectral similarity of the normalized Laplacians. This promotes agreement between the clustering structure and diffusion properties of the learned features and masked predictions.*

PAC-Bayesian view of structural regularization. We now present a PAC-Bayesian view of GCR, which bounds generalization by linking expected loss to empirical loss and the divergence between posterior and prior over hypotheses.

Let \mathcal{P} denote a prior distribution over model functions f , representing a structure-agnostic belief (e.g., uniform or isotropic Gaussian over parameters). Let \mathcal{Q} be a posterior distribution supported on models that minimize training loss while also conforming to a structural constraint induced by GCR, i.e., \mathcal{Q} is restricted to functions f such that $\mathcal{L}_{\text{GCR}}^{(l)} \leq \epsilon$ for each relevant layer l .

Theorem 2 (PAC-Bayes generalization bound with GCR). *Let $\mathcal{L}(f) = \mathbb{E}_{(x,y) \sim \mathcal{D}}[\ell(f(x), y)]$ be the expected population loss of model f and let $\hat{\mathcal{L}}(f) = \frac{1}{n} \sum_{i=1}^n \ell(f(x_i), y_i)$ be the empirical loss on n training examples. Then, for any posterior distribution \mathcal{Q} over functions and any prior distribution \mathcal{P} , with probability at least $1 - \delta$ over the training data, the following bound holds:*

$$\mathbb{E}_{f \sim \mathcal{Q}}[\mathcal{L}(f)] \leq \mathbb{E}_{f \sim \mathcal{Q}}[\hat{\mathcal{L}}(f)] + \sqrt{\frac{\text{KL}(\mathcal{Q} \parallel \mathcal{P}) + \log(1/\delta)}{2n}}. \quad (14)$$

This classical PAC-Bayesian bound quantifies generalization through two factors: (i) the empirical performance of models sampled from the posterior \mathcal{Q} , and (ii) the Kullback-Leibler (KL) divergence[44] $\text{KL}(\mathcal{Q} \parallel \mathcal{P})$, measuring how much \mathcal{Q} deviates from the prior. In GCR, the constraint $\mathcal{L}_{\text{GCR}}^{(l)} \leq \epsilon$ imposes structured alignment between feature similarity $\mathbf{F}^{(l)}$ and semantic prediction structure \mathbf{P} , serving as an inductive bias. Thus, when \mathcal{Q} is supported on models satisfying this constraint, the KL complexity term reflects the strength of this alignment.

Proposition 2 (Structure-induced KL complexity). *If the posterior \mathcal{Q} is concentrated on models with small GCR loss at layer l , then the KL divergence to an isotropic prior \mathcal{P} satisfies:*

$$\text{KL}(\mathcal{Q} \parallel \mathcal{P}) \leq C \sum_l \|\mathbf{F}^{(l)} - \mathbf{P}\|_F^2, \quad (15)$$

for some constant C depending on the form of \mathcal{P} .

Proof. The proof can be found in Appendix E. \square

Remark 2. *This perspective shows that GCR does more than minimize training loss, it also implicitly regularizes the hypothesis space by favoring models whose internal representations reflect known semantic structure. This improves generalization by reducing the effective size of the model class, as made explicit through the PAC-Bayesian framework.*

4 Experiment

4.1 Datasets, Models, and Experimental Setup

We evaluate GCR on several benchmark datasets, including Kaggle cats vs. dogs[22], CIFAR-10[62], CIFAR-100[62], Tiny ImageNet[63], and ImageNet-1K [23]. Our evaluation spans a di-

Table 2: Accuracy (%) on CIFAR-100 across models.

	MAE	MNet	SN	SQNet	Rx-50	Rx-101	R34	R50	D121	Mean
Baseline	64.29 \pm 0.34	65.95 \pm 0.25	70.11 \pm 0.30	69.43 \pm 0.27	77.75 \pm 0.29	77.83 \pm 0.30	76.82 \pm 0.28	77.31 \pm 0.29	77.09 \pm 0.27	72.95 \pm 5.50
Early GCL	65.05 \pm 0.29	67.45 \pm 0.21	71.96 \pm 0.27	70.90 \pm 0.20	79.18 \pm 0.22	79.69 \pm 0.27	77.90 \pm 0.22	79.37 \pm 0.25	79.41 \pm 0.22	74.55 \pm 5.78
Mid GCL	64.99 \pm 0.30	67.88 \pm 0.21	71.89 \pm 0.24	70.21 \pm 0.25	79.07 \pm 0.19	79.28 \pm 0.26	77.83 \pm 0.20	78.90 \pm 0.24	79.26 \pm 0.21	74.37 \pm 5.66
Late GCL	65.54 \pm 0.27	68.32 \pm 0.20	71.42 \pm 0.24	70.55 \pm 0.22	79.54 \pm 0.20	79.83 \pm 0.21	78.31 \pm 0.20	79.42 \pm 0.21	79.69 \pm 0.23	74.74 \pm 5.73
Early+Mid	65.23 \pm 0.31	67.62 \pm 0.24	71.50 \pm 0.28	70.47 \pm 0.19	78.90 \pm 0.18	79.25 \pm 0.20	77.41 \pm 0.19	78.58 \pm 0.24	79.22 \pm 0.20	74.28 \pm 5.56
Mid+Late	65.27 \pm 0.28	68.33 \pm 0.19	71.63 \pm 0.28	70.30 \pm 0.22	78.91 \pm 0.17	79.57 \pm 0.21	77.30 \pm 0.20	78.85 \pm 0.22	79.54 \pm 0.24	74.41 \pm 5.55
Early+Late	65.22 \pm 0.21	67.25 \pm 0.21	71.55 \pm 0.27	71.03 \pm 0.24	79.03 \pm 0.20	79.41 \pm 0.22	78.19 \pm 0.23	78.70 \pm 0.23	79.45 \pm 0.22	74.43 \pm 5.69
Full GCL	65.38 \pm 0.22	68.22 \pm 0.19	71.30 \pm 0.24	70.77 \pm 0.20	79.01 \pm 0.19	79.29 \pm 0.21	77.79 \pm 0.20	78.71 \pm 0.22	79.27 \pm 0.19	74.42 \pm 5.49

Table 3: Accuracy (%) on Tiny ImageNet across models. All results are obtained by training models from scratch. We also evaluate Stochastic ResNet-18 (R18SD) and SE-ResNet-18 (SER18).

	ViT ₃₂	ViT ₁₆	CeIT	MViT _{XXS}	MViT _{XS}	MViT	Swin	MNet	R18SD	SER18	R34	Mean
Baseline	37.79 \pm 0.35	40.05 \pm 0.33	49.95 \pm 0.29	49.28 \pm 0.29	51.58 \pm 0.27	52.68 \pm 0.27	54.27 \pm 0.25	57.81 \pm 0.25	63.49 \pm 0.26	65.65 \pm 0.24	67.51 \pm 0.25	53.64 \pm 9.62
Early GCL	39.02 \pm 0.29	40.98 \pm 0.19	51.22 \pm 0.20	50.11 \pm 0.28	51.33 \pm 0.26	53.91 \pm 0.22	54.88 \pm 0.25	57.93 \pm 0.21	63.81 \pm 0.19	66.52 \pm 0.22	67.79 \pm 0.19	54.32 \pm 9.39
Mid GCL	38.61 \pm 0.23	40.95 \pm 0.19	50.30 \pm 0.19	49.92 \pm 0.26	51.43 \pm 0.22	53.88 \pm 0.20	55.23 \pm 0.24	57.63 \pm 0.20	64.03 \pm 0.22	65.66 \pm 0.23	67.62 \pm 0.20	54.11 \pm 9.38
Late GCL	37.98 \pm 0.28	40.35 \pm 0.25	50.82 \pm 0.20	49.77 \pm 0.21	51.99 \pm 0.23	54.10 \pm 0.19	55.47 \pm 0.21	57.87 \pm 0.23	63.79 \pm 0.19	65.85 \pm 0.25	67.61 \pm 0.19	54.18 \pm 9.56
Early+Mid	39.08 \pm 0.25	41.26 \pm 0.18	50.25 \pm 0.25	49.73 \pm 0.22	51.57 \pm 0.19	53.91 \pm 0.23	54.95 \pm 0.19	57.49 \pm 0.19	64.18 \pm 0.20	65.86 \pm 0.24	67.74 \pm 0.23	54.18 \pm 9.32
Mid+Late	38.44 \pm 0.18	40.52 \pm 0.28	50.09 \pm 0.25	50.55 \pm 0.18	51.48 \pm 0.21	53.90 \pm 0.20	55.62 \pm 0.23	57.65 \pm 0.21	64.29 \pm 0.17	65.95 \pm 0.19	67.58 \pm 0.21	54.19 \pm 9.52
Early+Late	38.34 \pm 0.23	40.71 \pm 0.21	50.70 \pm 0.25	50.23 \pm 0.20	51.36 \pm 0.18	53.57 \pm 0.21	54.89 \pm 0.21	57.93 \pm 0.19	63.88 \pm 0.19	65.83 \pm 0.17	67.72 \pm 0.25	54.11 \pm 9.47
Full GCL	38.38 \pm 0.22	40.80 \pm 0.18	49.92 \pm 0.20	50.16 \pm 0.17	51.87 \pm 0.19	54.01 \pm 0.19	54.87 \pm 0.19	57.64 \pm 0.20	64.10 \pm 0.19	66.01 \pm 0.15	67.66 \pm 0.18	54.13 \pm 9.49

verse range of architectures, from lightweight models (*e.g.*, MobileNet[46], ShuffleNet[124], and SqueezeNet[51]), to deeper CNNs (*e.g.*, GoogLeNet[97], ResNet[42], DenseNet[48], ResNeXt[112], Stochastic ResNet[49], and SE-ResNet[47]). We also include transformer-based architectures such as ViT[31], Swin[70], MobileViT[77], CEiT[120]), iFormer [95], ViG [37], as well as Masked Autoencoders (MAE) [41].

Experiments run on NVIDIA V100 GPUs with 12 CPUs and 48 GB RAM. For CNNs, we follow [25]: 200 epochs, initial learning rate 0.1 (decayed at epochs 60/120/160), batch size 128, weight decay 5×10^{-4} , and momentum 0.9. For transformers, we use AdamW with a learning rate of 1×10^{-4} , cosine annealing, weight decay 5×10^{-2} , batch size 256, AMP[30], 10-epoch warm-up, and gradient clipping (norm 1.0). We divide each model into three stages: early (E), middle (M), and late (L), and insert GCLs to create seven configurations: individual stages (E, M or L), pairs (E+M, M+L, E+L), and full GCL. We evaluate weighting schemes including equal, linear, square root, squared, cosine, arccosine, and adaptive. All experiments use $\lambda = 1$. We report the mean and standard deviation over 10 runs for CIFAR-10, CIFAR-100, and Tiny ImageNet, and over 3 runs for ImageNet-1K.

Appendix F presents a detailed analysis of GCR’s time complexity, while Appendix G provides complete details of the experimental setup.

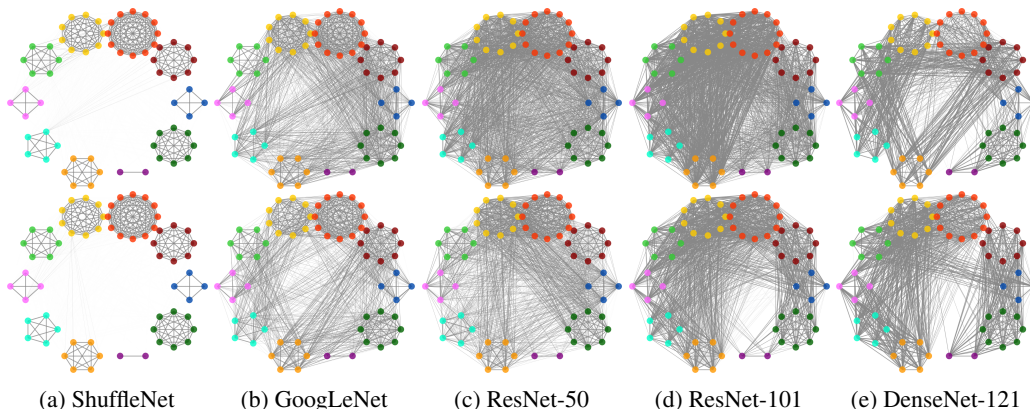


Figure 5: Relational graph comparison across five models on the same batch. Top row: baselines; bottom row: GCL-augmented versions, showing *sparser inter-class connections* and *stronger class-aware structure*, highlighting GCL’s effectiveness in enhancing relational representations.

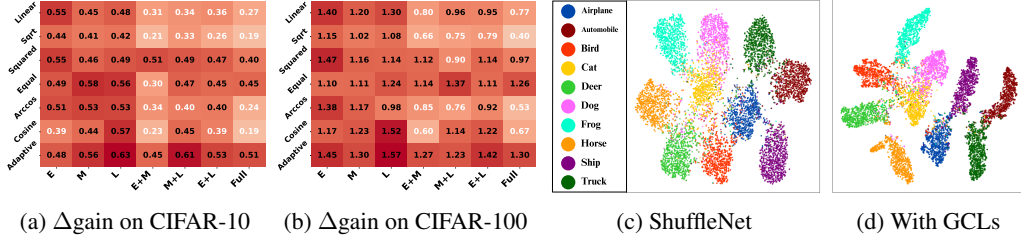


Figure 6: Performance gains (Δ ,%) from adding GCLs with different configurations across various weighting schemes. Darker red indicates larger gains. Adaptive weighting achieves the highest improvement, showing the value of graph misalignment as a guidance signal. (c) and (d) show that GCL-augmented ShuffleNet yields more compact intra-class clusters and better inter-class separation.

4.2 Quantitative and Qualitative Evaluation

GCL can serve as an attention mechanism. Fig. 3 offers a visual comparison between feature activations from a baseline CNN model and those from a GCL-augmented model, both trained on identical data batches. The key distinction lies in the sharper, more localized activations produced by the GCL-enhanced model. Notably, the parameter-free GCL mechanism yields feature maps that are more aligned with semantically relevant regions, such as the eyes, ears, and facial outlines of the cat, and the tongue, snout, and eyes of the dog. This suggests that GCL encourages the network to focus on class-discriminative features, thereby reducing attention to background or irrelevant image regions. In contrast, the baseline model’s activations appear diffuse and less structured, indicating weaker spatial selectivity. The visual improvements align well with the reported jump in classification accuracy from 98.1% to 99.8%, highlighting that improved interpretability does not come at the cost of performance, rather, it appears to enhance it. Fig. 4 compares how GCLs guide model learning.

GCLs lead to more interpretable and discriminative feature spaces. In GCL-augmented graphs (Figs. 1 and 5), semantically similar classes such as Airplane, Ship, and Truck (all vehicles) form closer associations, suggesting that GCL helps the model better understand high-level concepts. A similar trend appears among animal-related classes (e.g., Dog, Cat, Horse, and Deer). As model complexity increases (from ShuffleNet to DenseNet-121), the relational graphs become denser. However, GCL still consistently improves clarity. Even in large-capacity models like ResNet-101 and DenseNet-121, GCL enhances structure by reducing cross-class noise and reinforcing class-wise coherence. The consistent improvements across very different models, from lightweight ShuffleNet to deep DenseNet, demonstrate the general applicability of GCL. It does not merely overfit to a specific architecture but contributes to relational learning in a model-agnostic, parameter-free way.

Adaptive weighting and selective layers boost GCR effectiveness. The adaptive scheme consistently yields the highest or near-highest gains (Figs. 6a and 6b), especially on CIFAR-100, where deeper features benefit more from dynamic supervision. Placing GCLs at later layers (L) or in combinations involving deeper blocks (e.g., E+L, Full) yields the greatest improvements, highlighting the semantic richness of deeper layers. Among fixed schemes, squared and equal weighting outperform linear. Notably, applying GCLs to all layers (Full) does not always yield the best gains, indicating that naïve aggregation can weaken the regularization effect. These findings emphasize the value of selective layer placement and adaptive weighting to effectively guide feature alignment.

Tables 1, 2, and 3 summarize the accuracy gains achieved by GCR across three benchmarks.

GCLs are effective across various datasets and model types. Across CIFAR-10, CIFAR-100, and Tiny ImageNet, GCR consistently improves accuracy relative to the baseline in nearly all configurations. On CIFAR-10, which is comparatively simpler, GCR delivers a peak mean accuracy of 94.07% (Late GCL), improving over the 93.32% baseline. CIFAR-100, with greater semantic granularity and inter-class overlap, benefits even more: Late GCL increases the mean accuracy from 72.95% to 74.74%, a +1.79% absolute gain. On Tiny ImageNet, where models are trained from scratch under more challenging conditions, GCR again proves effective. The best performance is achieved with Early GCL (54.32%) and Late GCL (54.18%), improving over the 53.64% baseline and affirming GCR’s applicability to both convolutional and transformer-based vision models.

Table 4: Comparison of iFormer, ViT, and ViG with different GCL integration strategies on ImageNet-1K. Results are averaged over three runs.

Method	iFormer-S	iFormer-B	ViT-B/16	ViG-B
Baseline	83.4 \pm 0.40	84.6 \pm 0.45	74.3 \pm 0.51	82.3 \pm 0.42
Early GCL	83.8 \pm 0.31	85.0 \pm 0.40	74.7 \pm 0.44	82.8 \pm 0.35
Mid GCL	83.8 \pm 0.39	85.5 \pm 0.33	75.2 \pm 0.36	83.0 \pm 0.34
Late GCL	84.5 \pm 0.29	86.1 \pm 0.30	75.8 \pm 0.33	84.0 \pm 0.30
Early + Mid	84.3 \pm 0.33	85.9 \pm 0.38	75.6 \pm 0.41	83.7 \pm 0.33
Mid + Late	84.8 \pm 0.28	85.9 \pm 0.37	75.6 \pm 0.34	83.9 \pm 0.30
Early + Late	84.5 \pm 0.30	85.2 \pm 0.28	74.9 \pm 0.33	83.5 \pm 0.29
Full GCL	84.3 \pm 0.29	85.8 \pm 0.26	75.5 \pm 0.30	83.6 \pm 0.27

GCLs improve transformer architectures on ImageNet-1K. We conducted experiments on ImageNet-1K using transformer-based architectures (*e.g.*, iFormer, ViT, and ViG). Results are summarized in Table 4. Key results demonstrate the effectiveness of our approach. For iFormer-S, GCR boosts performance from 83.4% to 84.8%, yielding a +1.4% gain. For iFormer-B, accuracy improves from 84.6% to 86.1%, corresponding to a +1.5% gain. Similar improvements are also observed with ViT-B/16 and ViG-B, confirming the generality of our method. These improvements validate that GCR scales effectively to large, complex datasets and modern architectures. They support our core hypothesis: aligning feature geometry with prediction semantics enhances generalization. Moreover, GCR achieves this without architectural changes or added parameters, reinforcing its value as a model-agnostic and lightweight regularizer.

GCLs are most effective in later layers, aligning with decision structures. Among GCL configurations, those applied at later stages generally yield the most significant improvements. Late GCL consistently achieves the highest or near-highest performance across all three datasets. This is likely because later layers encode higher-level semantic representations that align more closely with class-level decision boundaries. Aligning these representations with the prediction graph enhances inter-class separability while reducing intra-class dispersion, especially on fine-grained tasks like CIFAR-100 and Tiny ImageNet. While Early and Mid GCLs also contribute, their benefits are comparatively moderate, indicating that feature regularization at earlier stages may be less semantically meaningful or more susceptible to noise. Figs. 6a and 6b show clear performance gains.

GCLs enhance geometry and generalization. Finally, the results substantiate GCR’s central hypothesis: aligning feature space geometry with the model’s own prediction space fosters more discriminative and generalizable representations. Across datasets, GCR reduces classification ambiguity, tightens intra-class cohesion, and sharpens class boundaries, particularly important in datasets with high inter-class similarity. Figs. 6c and 6d compare results on ShuffleNet, showing that the GCL-augmented model produces more compact intra-class clusters and better inter-class separability. Moreover, GCR achieves this with minimal computational overhead and zero parameter increase, making it highly practical for real-world deployment where architectural changes or expensive training adjustments are undesirable.

Additional results, visualizations, and discussions are provided in Appendix H, while the work’s limitations and future research directions are covered in Appendix I.

5 Conclusion

We introduced GCR, a novel approach for enhancing classification by aligning the structural relationships between feature representations and model predictions through parameter-free, modular GCLs. By constructing feature relational graphs at multiple points in the network and aligning them with a global masked prediction graph, GCR encourages the network to learn semantically meaningful and class-consistent representations. This graph-based alignment acts as a form of neural network prompting, guiding learning without modifying the architecture or training procedure. Our experiments across diverse architectures demonstrate that GCR improves intra-class cohesion, reduces noisy inter-class similarity, and leads to better generalization. We believe this work offers a new perspective on structured representation learning by using prediction structure as a regularizing signal. Future work may explore extending this idea to tasks beyond classification, such as segmentation or retrieval, and integrating it with self-supervised learning frameworks.

Acknowledgments and Disclosure of Funding

Xi Ding, a visiting scholar at the ARC Research Hub for Driving Farming Productivity and Disease Prevention, Griffith University, conducted this work under the supervision of Lei Wang.

We sincerely thank the anonymous reviewers for their invaluable insights and constructive feedback, which have greatly contributed to improving our work.

This work was supported by the Australian Research Council (ARC) under Industrial Transformation Research Hub Grant IH180100002.

This work was also supported by computational resources provided by the Australian Government through the National Computational Infrastructure (NCI) under both the ANU Merit Allocation Scheme and the CSIRO Allocation Scheme.

References

- [1] T. Agouti. Graph-based modeling using association rule mining to detect influential users in social networks. *Expert Systems with Applications*, 202:117436, 2022.
- [2] G. Aguilar, Y. Ling, Y. Zhang, B. Yao, X. Fan, and C. Guo. Knowledge distillation from internal representations. In *Proceedings of the AAAI conference on artificial intelligence*, volume 34, pages 7350–7357, 2020.
- [3] I. Alonso, A. Sabater, D. Ferstl, L. Montesano, and A. C. Murillo. Semi-supervised semantic segmentation with pixel-level contrastive learning from a class-wise memory bank. In *Proceedings of the IEEE/CVF international conference on computer vision*, pages 8219–8228, 2021.
- [4] R. Ando and T. Zhang. Learning on graph with laplacian regularization. *Advances in neural information processing systems*, 19, 2006.
- [5] F. Bauer. Normalized graph laplacians for directed graphs. *Linear Algebra and its Applications*, 436(11):4193–4222, 2012.
- [6] M. Belkin and P. Niyogi. Laplacian eigenmaps for dimensionality reduction and data representation. *Neural computation*, 15(6):1373–1396, 2003.
- [7] M. Belkin, P. Niyogi, and V. Sindhwani. Manifold regularization: A geometric framework for learning from labeled and unlabeled examples. *Journal of machine learning research*, 7(11), 2006.
- [8] M. M. Bronstein, J. Bruna, Y. LeCun, A. Szlam, and P. Vandergheynst. Geometric deep learning: going beyond euclidean data. *IEEE Signal Processing Magazine*, 34(4):18–42, 2017.
- [9] A. Bulat, E. Sánchez-Lozano, and G. Tzimiropoulos. Improving memory banks for unsupervised learning with large mini-batch, consistency and hard negative mining. In *ICASSP 2021-2021 IEEE International Conference on Acoustics, Speech and Signal Processing (ICASSP)*, pages 1695–1699. IEEE, 2021.
- [10] I. Chami, Z. Ying, C. Ré, and J. Leskovec. Hyperbolic graph convolutional neural networks. *Advances in neural information processing systems*, 32, 2019.
- [11] C. Chen, Z. Wang, J. Wu, X. Wang, L.-Z. Guo, Y.-F. Li, and S. Liu. Interactive graph construction for graph-based semi-supervised learning. *IEEE Transactions on Visualization and Computer Graphics*, 27(9):3701–3716, 2021.
- [12] Q. Chen, L. Wang, P. Koniusz, and T. Gedeon. Motion meets attention: Video motion prompts. In *The 16th Asian Conference on Machine Learning (Conference Track)*, 2024.
- [13] R. Chen, S. Zhang, Y. Li, et al. Redundancy-free message passing for graph neural networks. *Advances in Neural Information Processing Systems*, 35:4316–4327, 2022.

- [14] T. Chen, S. Kornblith, M. Norouzi, and G. Hinton. A simple framework for contrastive learning of visual representations. In *International conference on machine learning*, pages 1597–1607. PmLR, 2020.
- [15] T. Chen, C. Luo, and L. Li. Intriguing properties of contrastive losses. *Advances in Neural Information Processing Systems*, 34:11834–11845, 2021.
- [16] Y. Chen, M. Rohrbach, Z. Yan, Y. Shuicheng, J. Feng, and Y. Kalantidis. Graph-based global reasoning networks. In *Proceedings of the IEEE/CVF conference on computer vision and pattern recognition*, pages 433–442, 2019.
- [17] Y. Chen, Z. Yang, Y. Xie, and Z. Wang. Contrastive learning from pairwise measurements. *Advances in Neural Information Processing Systems*, 31, 2018.
- [18] H. Choi, A. Som, and P. Turaga. Amc-loss: Angular margin contrastive loss for improved explainability in image classification. In *Proceedings of the IEEE/CVF conference on computer vision and pattern recognition workshops*, pages 838–839, 2020.
- [19] C.-Y. Chuang, J. Robinson, Y.-C. Lin, A. Torralba, and S. Jegelka. Debaised contrastive learning. *Advances in neural information processing systems*, 33:8765–8775, 2020.
- [20] E. Cole, X. Yang, K. Wilber, O. Mac Aodha, and S. Belongie. When does contrastive visual representation learning work? In *Proceedings of the IEEE/CVF conference on computer vision and pattern recognition*, pages 14755–14764, 2022.
- [21] X. S. Cuadros, L. Zappella, and N. Apostoloff. Self-conditioning pre-trained language models. In *International Conference on Machine Learning*, pages 4455–4473. PMLR, 2022.
- [22] W. Cukierski. Dogs vs. cats. <https://kaggle.com/competitions/dogs-vs-cats>, 2013. Kaggle.
- [23] J. Deng, W. Dong, R. Socher, L.-J. Li, K. Li, and L. Fei-Fei. Imagenet: A large-scale hierarchical image database. In *2009 IEEE conference on computer vision and pattern recognition*, pages 248–255. Ieee, 2009.
- [24] W. Deng, L. Zheng, Y. Sun, and J. Jiao. Rethinking triplet loss for domain adaptation. *IEEE Transactions on Circuits and Systems for Video Technology*, 31:29–37, 2020.
- [25] T. DeVries and G. W. Taylor. Improved regularization of convolutional neural networks with cutout. *arXiv preprint arXiv:1708.04552*, 2017.
- [26] X. Ding and L. Wang. Do language models understand time? *arXiv preprint arXiv:2412.13845*, 2024.
- [27] X. Ding and L. Wang. Quo vadis, anomaly detection? llms and vlms in the spotlight. *arXiv preprint arXiv:2412.18298*, 2024.
- [28] X. Ding and L. Wang. The journey of action recognition. In *Companion Proceedings of the ACM Web Conference 2025, WWW '25 Companion*, New York, NY, USA, 2025. Association for Computing Machinery.
- [29] T.-T. Do, T. Tran, I. D. Reid, B. V. Kumar, T. Hoang, and G. Carneiro. A theoretically sound upper bound on the triplet loss for improving the efficiency of deep distance metric learning. *2019 IEEE/CVF Conference on Computer Vision and Pattern Recognition (CVPR)*, pages 10396–10405, 2019.
- [30] M. Dörrich, M. Fan, and A. M. Kist. Impact of mixed precision techniques on training and inference efficiency of deep neural networks. *IEEE Access*, 11:57627–57634, 2023.
- [31] A. Dosovitskiy, L. Beyer, A. Kolesnikov, D. Weissenborn, X. Zhai, T. Unterthiner, M. Dehghani, M. Minderer, G. Heigold, S. Gelly, et al. An image is worth 16x16 words: Transformers for image recognition at scale. *arXiv preprint arXiv:2010.11929*, 2020.
- [32] R. M. Dudley. Metric entropy of some classes of sets with differentiable boundaries. *Journal of Approximation Theory*, 10(3):227–236, 1974.

- [33] V. P. Dwivedi, C. K. Joshi, A. T. Luu, T. Laurent, Y. Bengio, and X. Bresson. Benchmarking graph neural networks. *Journal of Machine Learning Research*, 24(43):1–48, 2023.
- [34] L. Fan, S. Liu, P.-Y. Chen, G. Zhang, and C. Gan. When does contrastive learning preserve adversarial robustness from pretraining to finetuning? *Advances in neural information processing systems*, 34:21480–21492, 2021.
- [35] P. Germain, F. Bach, A. Lacoste, and S. Lacoste-Julien. Pac-bayesian theory meets bayesian inference. *Advances in Neural Information Processing Systems*, 29, 2016.
- [36] F. Guo, R. He, J. Dang, and J. Wang. Working memory-driven neural networks with a novel knowledge enhancement paradigm for implicit discourse relation recognition. In *Proceedings of the AAAI Conference on Artificial Intelligence*, volume 34, pages 7822–7829, 2020.
- [37] K. Han, Y. Wang, J. Guo, Y. Tang, and E. Wu. Vision gnn: An image is worth graph of nodes. *Advances in neural information processing systems*, 35:8291–8303, 2022.
- [38] L. Han, X. Jiaying, N. Jinjie, and K. Yiping. Rethinking the message passing for graph-level classification tasks in a category-based view. *Engineering Applications of Artificial Intelligence*, 143:109897, 2025.
- [39] T. Han, W.-W. Tu, and Y.-F. Li. Explanation consistency training: Facilitating consistency-based semi-supervised learning with interpretability. In *AAAI Conference on Artificial Intelligence*, 2021.
- [40] H. He, A. Kosasih, X. Yu, J. Zhang, S. Song, W. Hardjawana, and K. B. Letaief. Gnn-enhanced approximate message passing for massive/ultra-massive mimo detection. In *2023 IEEE Wireless Communications and Networking Conference (WCNC)*, pages 1–6. IEEE, 2023.
- [41] K. He, X. Chen, S. Xie, Y. Li, P. Dollár, and R. Girshick. Masked autoencoders are scalable vision learners. In *Proceedings of the IEEE/CVF conference on computer vision and pattern recognition*, pages 16000–16009, 2022.
- [42] K. He, X. Zhang, S. Ren, and J. Sun. Deep residual learning for image recognition. In *Proceedings of the IEEE conference on computer vision and pattern recognition*, pages 770–778, 2016.
- [43] T. He, Y. Zhang, K. Ren, M. Liu, C. Wang, W. Zhang, Y. Yang, and D. Li. Reinforcement learning with automated auxiliary loss search. *Advances in neural information processing systems*, 35:1820–1834, 2022.
- [44] J. R. Hershey and P. A. Olsen. Approximating the kullback leibler divergence between gaussian mixture models. In *2007 IEEE International Conference on Acoustics, Speech and Signal Processing-ICASSP'07*, volume 4, pages IV–317. IEEE, 2007.
- [45] C.-H. Ho and N. Nvasconcelos. Contrastive learning with adversarial examples. *Advances in Neural Information Processing Systems*, 33:17081–17093, 2020.
- [46] A. G. Howard. Mobilenets: Efficient convolutional neural networks for mobile vision applications. *arXiv preprint arXiv:1704.04861*, 2017.
- [47] J. Hu, L. Shen, and G. Sun. Squeeze-and-excitation networks. In *Proceedings of the IEEE conference on computer vision and pattern recognition*, pages 7132–7141, 2018.
- [48] G. Huang, Z. Liu, L. Van Der Maaten, and K. Q. Weinberger. Densely connected convolutional networks. In *Proceedings of the IEEE conference on computer vision and pattern recognition*, pages 4700–4708, 2017.
- [49] G. Huang, Y. Sun, Z. Liu, D. Sedra, and K. Q. Weinberger. Deep networks with stochastic depth. In *Computer Vision–ECCV 2016: 14th European Conference, Amsterdam, The Netherlands, October 11–14, 2016, Proceedings, Part IV 14*, pages 646–661. Springer, 2016.
- [50] Z. Huang, Y. Zou, B. Kumar, and D. Huang. Comprehensive attention self-distillation for weakly-supervised object detection. *Advances in neural information processing systems*, 33:16797–16807, 2020.

- [51] F. N. Iandola, S. Han, M. W. Moskewicz, K. Ashraf, W. J. Dally, and K. Keutzer. Squeezenet: Alexnet-level accuracy with 50x fewer parameters and < 0.5 mb model size. *arXiv preprint arXiv:1602.07360*, 2016.
- [52] A. A. Ismail, H. C. Bravo, and S. Feizi. Improving deep learning interpretability by saliency guided training. In *Neural Information Processing Systems*, 2021.
- [53] D. Jiang, Z. Wu, C.-Y. Hsieh, G. Chen, B. Liao, Z. Wang, C. Shen, D. Cao, J. Wu, and T. Hou. Could graph neural networks learn better molecular representation for drug discovery? a comparison study of descriptor-based and graph-based models. *Journal of cheminformatics*, 13:1–23, 2021.
- [54] W. Jiang. Graph-based deep learning for communication networks: A survey. *Computer Communications*, 185:40–54, 2022.
- [55] M. Jin, V. Khattar, H. Kaushik, B. Sel, and R. Jia. On solution functions of optimization: Universal approximation and covering number bounds. In *Proceedings of the AAAI Conference on Artificial Intelligence*, volume 37, pages 8123–8131, 2023.
- [56] J. Kang, R. Fernandez-Beltran, D. Hong, J. Chanussot, and A. Plaza. Graph relation network: Modeling relations between scenes for multilabel remote-sensing image classification and retrieval. *IEEE Transactions on Geoscience and Remote Sensing*, 59(5):4355–4369, 2020.
- [57] I. Kansizoglou, L. Bampis, and A. Gasteratos. Deep feature space: A geometrical perspective. *IEEE Transactions on Pattern Analysis and Machine Intelligence*, 44(10):6823–6838, 2021.
- [58] A. Kar, S. K. Dhara, D. Sen, and P. K. Biswas. Self-supervision via controlled transformation and unpaired self-conditioning for low-light image enhancement. *IEEE Transactions on Instrumentation and Measurement*, 2024.
- [59] M. A. Khamis, H. Q. Ngo, X. Nguyen, D. Olteanu, and M. Schleich. Learning models over relational data using sparse tensors and functional dependencies. *ACM Transactions on Database Systems (TODS)*, 45:1 – 66, 2017.
- [60] P. Khosla, P. Teterwak, C. Wang, A. Sarna, Y. Tian, P. Isola, A. Maschinot, C. Liu, and D. Krishnan. Supervised contrastive learning. *Advances in neural information processing systems*, 33:18661–18673, 2020.
- [61] T. N. Kipf and M. Welling. Semi-supervised classification with graph convolutional networks. *arXiv preprint arXiv:1609.02907*, 2016.
- [62] A. Krizhevsky, G. Hinton, et al. Learning multiple layers of features from tiny images. 2009.
- [63] Y. Le and X. Yang. Tiny imagenet visual recognition challenge. *CS 231N*, 7(7):3, 2015.
- [64] B. Li, Y. Li, and K. W. Eliceiri. Dual-stream multiple instance learning network for whole slide image classification with self-supervised contrastive learning. In *Proceedings of the IEEE/CVF conference on computer vision and pattern recognition*, pages 14318–14328, 2021.
- [65] P. Li, X. Yu, H. Peng, Y. Xian, L. Wang, L. Sun, J. Zhang, and P. S. Yu. Relational prompt-based pre-trained language models for social event detection. *ACM Transactions on Information Systems*, 43(1):1–43, 2024.
- [66] S. Li, X. Xia, S. Ge, and T. Liu. Selective-supervised contrastive learning with noisy labels. In *Proceedings of the IEEE/CVF conference on computer vision and pattern recognition*, pages 316–325, 2022.
- [67] P. Liu, W. Yuan, J. Fu, Z. Jiang, H. Hayashi, and G. Neubig. Pre-train, prompt, and predict: A systematic survey of prompting methods in natural language processing. *ACM computing surveys*, 55(9):1–35, 2023.
- [68] Q. Liu and S. Mukhopadhyay. Unsupervised learning using pretrained cnn and associative memory bank. In *2018 International Joint Conference on Neural Networks (IJCNN)*, pages 01–08. IEEE, 2018.

- [69] X. Liu, F. Zhang, Z. Hou, L. Mian, Z. Wang, J. Zhang, and J. Tang. Self-supervised learning: Generative or contrastive. *IEEE transactions on knowledge and data engineering*, 35(1):857–876, 2021.
- [70] Z. Liu, Y. Lin, Y. Cao, H. Hu, Y. Wei, Z. Zhang, S. Lin, and B. Guo. Swin transformer: Hierarchical vision transformer using shifted windows. In *Proceedings of the IEEE/CVF international conference on computer vision*, pages 10012–10022, 2021.
- [71] Z. Lu, Y. Sun, Z. Yang, Q. Zhou, and H. Lin. The orthogonality of weight vectors: The key characteristics of normalization and residual connections. In *International Joint Conference on Artificial Intelligence*, 2024.
- [72] R. Luo, Y. Wang, and Y. Wang. Rethinking the effect of data augmentation in adversarial contrastive learning. *arXiv preprint arXiv:2303.01289*, 2023.
- [73] Z. Luo, S. Cai, Y. Wang, and B. C. Ooi. Regularized pairwise relationship based analytics for structured data. *Proceedings of the ACM on Management of Data*, 1:1 – 27, 2023.
- [74] J. Ma, N. Wang, and B. Xiao. Semi-supervised classification with graph structure similarity and extended label propagation. *IEEE Access*, 7:58010–58022, 2019.
- [75] A. M. Mansourian, A. Jalali, R. Ahmadi, and S. Kasaei. Attention-guided feature distillation for semantic segmentation. *arXiv preprint arXiv:2403.05451*, 2024.
- [76] K. Marino, R. Salakhutdinov, and A. Gupta. The more you know: Using knowledge graphs for image classification. *arXiv preprint arXiv:1612.04844*, 2016.
- [77] S. Mehta and M. Rastegari. Mobilevit: light-weight, general-purpose, and mobile-friendly vision transformer. *arXiv preprint arXiv:2110.02178*, 2021.
- [78] R. Moradi, R. Berangi, and B. Minaei. A survey of regularization strategies for deep models. *Artificial Intelligence Review*, 53(6):3947–3986, 2020.
- [79] G. Nikolentzos, M. Thomas, A. R. Rivera, and M. Vazirgiannis. Image classification using graph-based representations and graph neural networks. In *Complex Networks & Their Applications IX: Volume 2, Proceedings of the Ninth International Conference on Complex Networks and Their Applications COMPLEX NETWORKS 2020*, pages 142–153. Springer, 2021.
- [80] J. Pang and G. Cheung. Graph laplacian regularization for image denoising: Analysis in the continuous domain. *IEEE Transactions on Image Processing*, 26(4):1770–1785, 2017.
- [81] V. Patel, V. Chaurasia, R. Mahadeva, and S. P. Patole. Garl-net: graph based adaptive regularized learning deep network for breast cancer classification. *IEEE Access*, 11:9095–9112, 2023.
- [82] L. Peel. Graph-based semi-supervised learning for relational networks. In *Proceedings of the 2017 SIAM international conference on data mining*, pages 435–443. SIAM, 2017.
- [83] C. Peng, X. Yang, K. E. Smith, Z. Yu, A. Chen, J. Bian, and Y. Wu. Model tuning or prompt tuning? a study of large language models for clinical concept and relation extraction. *Journal of biomedical informatics*, 153:104630, 2024.
- [84] F. Pernici, M. Bruni, C. Baecchi, and A. Bimbo. Maximally compact and separated features with regular polytope networks. *ArXiv*, abs/2301.06116, 2023.
- [85] P. E. Pope, S. Kolouri, M. Rostami, C. E. Martin, and H. Hoffmann. Explainability methods for graph convolutional neural networks. In *Proceedings of the IEEE/CVF conference on computer vision and pattern recognition*, pages 10772–10781, 2019.
- [86] C. Qi and F. Su. Contrastive-center loss for deep neural networks. In *2017 IEEE international conference on image processing (ICIP)*, pages 2851–2855. IEEE, 2017.
- [87] M. Rath and A. P. Condurache. Boosting deep neural networks with geometrical prior knowledge: A survey. *Artificial Intelligence Review*, 57(4):95, 2024.

- [88] W. Rawat and Z. Wang. Deep convolutional neural networks for image classification: A comprehensive review. *Neural computation*, 29(9):2352–2449, 2017.
- [89] E. Rossi, H. Kenlay, M. I. Gorinova, B. P. Chamberlain, X. Dong, and M. M. Bronstein. On the unreasonable effectiveness of feature propagation in learning on graphs with missing node features. In *Learning on graphs conference*, pages 11–1. PMLR, 2022.
- [90] U. Ruby, V. Yendapalli, et al. Binary cross entropy with deep learning technique for image classification. *Int. J. Adv. Trends Comput. Sci. Eng*, 9(10), 2020.
- [91] N. Saunshi, O. Plevrakis, S. Arora, M. Khodak, and H. Khandeparkar. A theoretical analysis of contrastive unsupervised representation learning. In *International Conference on Machine Learning*, pages 5628–5637. PMLR, 2019.
- [92] M. Schlichtkrull, T. N. Kipf, P. Bloem, R. Van Den Berg, I. Titov, and M. Welling. Modeling relational data with graph convolutional networks. In *The semantic web: 15th international conference, ESWC 2018, Heraklion, Crete, Greece, June 3–7, 2018, proceedings 15*, pages 593–607. Springer, 2018.
- [93] I. Sheth and S. E. Kahou. Auxiliary losses for learning generalizable concept-based models. In *Proceedings of the 37th International Conference on Neural Information Processing Systems, NIPS '23*, Red Hook, NY, USA, 2023. Curran Associates Inc.
- [94] Z. Shi, H. Wang, and C.-S. Leung. Constrained center loss for convolutional neural networks. *IEEE transactions on neural networks and learning systems*, 34(2):1080–1088, 2021.
- [95] C. Si, W. Yu, P. Zhou, Y. Zhou, X. Wang, and S. Yan. Inception transformer. *Advances in Neural Information Processing Systems*, 35:23495–23509, 2022.
- [96] Z. Song, X. Yang, Z. Xu, and I. King. Graph-based semi-supervised learning: A comprehensive review. *IEEE Transactions on Neural Networks and Learning Systems*, 34(11):8174–8194, 2022.
- [97] C. Szegedy, W. Liu, Y. Jia, P. Sermanet, S. Reed, D. Anguelov, D. Erhan, V. Vanhoucke, and A. Rabinovich. Going deeper with convolutions. In *Proceedings of the IEEE conference on computer vision and pattern recognition*, pages 1–9, 2015.
- [98] M. Tanveer, H.-K. Tan, H.-F. Ng, M. K. Leung, and J. H. Chuah. Regularization of deep neural network with batch contrastive loss. *IEEE Access*, 9:124409–124418, 2021.
- [99] Y. Tian, C. Sun, B. Poole, D. Krishnan, C. Schmid, and P. Isola. What makes for good views for contrastive learning? *Advances in neural information processing systems*, 33:6827–6839, 2020.
- [100] H. Touvron, M. Cord, M. Douze, F. Massa, A. Sablayrolles, and H. Jégou. Training data-efficient image transformers & distillation through attention. In *International conference on machine learning*, pages 10347–10357. PMLR, 2021.
- [101] V. Trivedy and L. J. Latecki. Cnn2graph: Building graphs for image classification. In *Proceedings of the IEEE/CVF Winter Conference on Applications of Computer Vision*, pages 1–11, 2023.
- [102] P. Veličković, G. Cucurull, A. Casanova, A. Romero, P. Lio, and Y. Bengio. Graph attention networks. *arXiv preprint arXiv:1710.10903*, 2017.
- [103] F. Wang and H. Liu. Understanding the behaviour of contrastive loss. In *Proceedings of the IEEE/CVF conference on computer vision and pattern recognition*, pages 2495–2504, 2021.
- [104] J. Wang, Y. Chen, R. Chakraborty, and S. X. Yu. Orthogonal convolutional neural networks. *2020 IEEE/CVF Conference on Computer Vision and Pattern Recognition (CVPR)*, pages 11502–11512, 2019.
- [105] P. Wang, K. Han, X.-S. Wei, L. Zhang, and L. Wang. Contrastive learning based hybrid networks for long-tailed image classification. In *Proceedings of the IEEE/CVF conference on computer vision and pattern recognition*, pages 943–952, 2021.

- [106] W. Wang, Y. Yang, X. Wang, W. Wang, and J. Li. Development of convolutional neural network and its application in image classification: a survey. *Optical Engineering*, 58(4):040901–040901, 2019.
- [107] X. Wang and G.-J. Qi. Contrastive learning with stronger augmentations. *IEEE transactions on pattern analysis and machine intelligence*, 45(5):5549–5560, 2022.
- [108] Y. Wang, Y. Deng, Y. Zheng, P. Chattopadhyay, and L. Wang. Vision transformers for image classification: A comparative survey. *Technologies*, 13(1):32, 2025.
- [109] Y. Wang, Y. Meng, Y. Li, S. Chen, Z. Fu, and H. Xue. Semi-supervised manifold regularization with adaptive graph construction. *Pattern Recognition Letters*, 98:90–95, 2017.
- [110] Z. Wen and Y. Li. Toward understanding the feature learning process of self-supervised contrastive learning. In *International Conference on Machine Learning*, pages 11112–11122. PMLR, 2021.
- [111] M. Wu, J. Zhou, Y. Peng, S. Wang, and Y. Zhang. Deep learning for image classification: a review. In *International Conference on Medical Imaging and Computer-Aided Diagnosis*, pages 352–362. Springer, 2023.
- [112] S. Xie, R. Girshick, P. Dollár, Z. Tu, and K. He. Aggregated residual transformations for deep neural networks. In *Proceedings of the IEEE conference on computer vision and pattern recognition*, pages 1492–1500, 2017.
- [113] T. Xie, B. Wang, and C.-C. J. Kuo. Graphhop: An enhanced label propagation method for node classification. *IEEE Transactions on Neural Networks and Learning Systems*, 34(11):9287–9301, 2022.
- [114] Y. Xie, Y. Liang, M. Gong, A. K. Qin, Y.-S. Ong, and T. He. Semisupervised graph neural networks for graph classification. *IEEE Transactions on Cybernetics*, 53(10):6222–6235, 2022.
- [115] Y. Xie, S. Lv, Y. Qian, C. Wen, and J. Liang. Active and semi-supervised graph neural networks for graph classification. *IEEE Transactions on Big Data*, 8(4):920–932, 2022.
- [116] L. Xu, J. Lian, W. X. Zhao, M. Gong, L. Shou, D. Jiang, X. Xie, and J.-R. Wen. Negative sampling for contrastive representation learning: A review. *arXiv preprint arXiv:2206.00212*, 2022.
- [117] S. S. Yadav and S. M. Jadhav. Deep convolutional neural network based medical image classification for disease diagnosis. *Journal of Big data*, 6(1):1–18, 2019.
- [118] J. Yin, H. Wu, and S. Sun. Effective sample pairs based contrastive learning for clustering. *Information Fusion*, 99:101899, 2023.
- [119] B. Yu and D. Tao. Deep metric learning with triplet margin loss. *2019 IEEE/CVF International Conference on Computer Vision (ICCV)*, pages 6489–6498, 2019.
- [120] K. Yuan, S. Guo, Z. Liu, A. Zhou, F. Yu, and W. Wu. Incorporating convolution designs into visual transformers. In *Proceedings of the IEEE/CVF international conference on computer vision*, pages 579–588, 2021.
- [121] D. Zhang, M. Cui, Y. Yang, P. Yang, C. Xie, D. Liu, B. Yu, and Z. Chen. Knowledge graph-based image classification refinement. *IEEE Access*, 7:57678–57690, 2019.
- [122] L. Zhang, X. Chen, J. Zhang, R. Dong, and K. Ma. Contrastive deep supervision. In *European Conference on Computer Vision*, pages 1–19. Springer, 2022.
- [123] T. Zhang. Covering number bounds of certain regularized linear function classes. *Journal of Machine Learning Research*, 2(Mar):527–550, 2002.
- [124] X. Zhang, X. Zhou, M. Lin, and J. Sun. Shufflenet: An extremely efficient convolutional neural network for mobile devices. In *Proceedings of the IEEE conference on computer vision and pattern recognition*, pages 6848–6856, 2018.

- [125] Y. Zhang, Q. Han, L. Wang, K. Cheng, B. Wang, and K. Zhan. Graph-weighted contrastive learning for semi-supervised hyperspectral image classification. *Journal of Electronic Imaging*, 34(2):023044–023044, 2025.
- [126] Y. Zhang, P. Tiño, A. Leonardis, and K. Tang. A survey on neural network interpretability. *IEEE Transactions on Emerging Topics in Computational Intelligence*, 5:726–742, 2020.
- [127] Y. Zhao, H. Wan, J. Gao, and Y. Lin. Improving relation classification by entity pair graph. In *Asian conference on machine learning*, pages 1156–1171. PMLR, 2019.
- [128] Z. Zhou, J. Liang, Y. Song, L. Yu, H. Wang, W. Zhang, Y. Yu, and Z. Zhang. Lipschitz generative adversarial nets. In K. Chaudhuri and R. Salakhutdinov, editors, *Proceedings of the 36th International Conference on Machine Learning*, volume 97 of *Proceedings of Machine Learning Research*, pages 7584–7593. PMLR, 09–15 Jun 2019.
- [129] Q. Zhu, B. Du, B. Turkbey, P. L. Choyke, and P. Yan. Deeply-supervised cnn for prostate segmentation. In *2017 international joint conference on neural networks (IJCNN)*, pages 178–184. IEEE, 2017.
- [130] X. Zhu, Z. Ghahramani, and J. D. Lafferty. Semi-supervised learning using gaussian fields and harmonic functions. In *Proceedings of the 20th International conference on Machine learning (ICML-03)*, pages 912–919, 2003.

NeurIPS Paper Checklist

i. Claims

Question: Do the main claims made in the abstract and introduction accurately reflect the paper's contributions and scope?

Answer: [Yes]

Justification: The abstract and introduction clearly state the claims made, including the contributions made in the paper and important assumptions and limitations.

Guidelines:

- The answer NA means that the abstract and introduction do not include the claims made in the paper.
- The abstract and/or introduction should clearly state the claims made, including the contributions made in the paper and important assumptions and limitations. A No or NA answer to this question will not be perceived well by the reviewers.
- The claims made should match theoretical and experimental results, and reflect how much the results can be expected to generalize to other settings.
- It is fine to include aspirational goals as motivation as long as it is clear that these goals are not attained by the paper.

ii. Limitations

Question: Does the paper discuss the limitations of the work performed by the authors?

Answer: [Yes]

Justification: Appendix I outlines the limitations of our approach and discusses potential directions for future work.

Guidelines:

- The answer NA means that the paper has no limitation while the answer No means that the paper has limitations, but those are not discussed in the paper.
- The authors are encouraged to create a separate "Limitations" section in their paper.
- The paper should point out any strong assumptions and how robust the results are to violations of these assumptions (e.g., independence assumptions, noiseless settings, model well-specification, asymptotic approximations only holding locally). The authors should reflect on how these assumptions might be violated in practice and what the implications would be.
- The authors should reflect on the scope of the claims made, e.g., if the approach was only tested on a few datasets or with a few runs. In general, empirical results often depend on implicit assumptions, which should be articulated.
- The authors should reflect on the factors that influence the performance of the approach. For example, a facial recognition algorithm may perform poorly when image resolution is low or images are taken in low lighting. Or a speech-to-text system might not be used reliably to provide closed captions for online lectures because it fails to handle technical jargon.
- The authors should discuss the computational efficiency of the proposed algorithms and how they scale with dataset size.
- If applicable, the authors should discuss possible limitations of their approach to address problems of privacy and fairness.
- While the authors might fear that complete honesty about limitations might be used by reviewers as grounds for rejection, a worse outcome might be that reviewers discover limitations that aren't acknowledged in the paper. The authors should use their best judgment and recognize that individual actions in favor of transparency play an important role in developing norms that preserve the integrity of the community. Reviewers will be specifically instructed to not penalize honesty concerning limitations.

iii. Theory assumptions and proofs

Question: For each theoretical result, does the paper provide the full set of assumptions and a complete (and correct) proof?

Answer: [Yes]

Justification: The proofs are provided in Appendix **D** and **E**.

Guidelines:

- The answer NA means that the paper does not include theoretical results.
- All the theorems, formulas, and proofs in the paper should be numbered and cross-referenced.
- All assumptions should be clearly stated or referenced in the statement of any theorems.
- The proofs can either appear in the main paper or the supplemental material, but if they appear in the supplemental material, the authors are encouraged to provide a short proof sketch to provide intuition.
- Inversely, any informal proof provided in the core of the paper should be complemented by formal proofs provided in appendix or supplemental material.
- Theorems and Lemmas that the proof relies upon should be properly referenced.

iv. **Experimental result reproducibility**

Question: Does the paper fully disclose all the information needed to reproduce the main experimental results of the paper to the extent that it affects the main claims and/or conclusions of the paper (regardless of whether the code and data are provided or not)?

Answer: [Yes]

Justification: Section **4.1** of the main paper and Appendix **G** provide comprehensive details necessary to reproduce our main experimental results. Additionally, we will release our code and pretrained models to support future research and facilitate further exploration of our approach.

Guidelines:

- The answer NA means that the paper does not include experiments.
- If the paper includes experiments, a No answer to this question will not be perceived well by the reviewers: Making the paper reproducible is important, regardless of whether the code and data are provided or not.
- If the contribution is a dataset and/or model, the authors should describe the steps taken to make their results reproducible or verifiable.
- Depending on the contribution, reproducibility can be accomplished in various ways. For example, if the contribution is a novel architecture, describing the architecture fully might suffice, or if the contribution is a specific model and empirical evaluation, it may be necessary to either make it possible for others to replicate the model with the same dataset, or provide access to the model. In general, releasing code and data is often one good way to accomplish this, but reproducibility can also be provided via detailed instructions for how to replicate the results, access to a hosted model (e.g., in the case of a large language model), releasing of a model checkpoint, or other means that are appropriate to the research performed.
- While NeurIPS does not require releasing code, the conference does require all submissions to provide some reasonable avenue for reproducibility, which may depend on the nature of the contribution. For example
 - (a) If the contribution is primarily a new algorithm, the paper should make it clear how to reproduce that algorithm.
 - (b) If the contribution is primarily a new model architecture, the paper should describe the architecture clearly and fully.
 - (c) If the contribution is a new model (e.g., a large language model), then there should either be a way to access this model for reproducing the results or a way to reproduce the model (e.g., with an open-source dataset or instructions for how to construct the dataset).
 - (d) We recognize that reproducibility may be tricky in some cases, in which case authors are welcome to describe the particular way they provide for reproducibility. In the case of closed-source models, it may be that access to the model is limited in some way (e.g., to registered users), but it should be possible for other researchers to have some path to reproducing or verifying the results.

v. **Open access to data and code**

Question: Does the paper provide open access to the data and code, with sufficient instructions to faithfully reproduce the main experimental results, as described in supplemental material?

Answer: [Yes]

Justification: Section 4.1 of the main paper and Appendix G provide comprehensive details necessary to reproduce our main experimental results. Additionally, we will release our code and pretrained models to support future research and facilitate further exploration of our approach.

Guidelines:

- The answer NA means that paper does not include experiments requiring code.
- Please see the NeurIPS code and data submission guidelines (<https://nips.cc/public/guides/CodeSubmissionPolicy>) for more details.
- While we encourage the release of code and data, we understand that this might not be possible, so “No” is an acceptable answer. Papers cannot be rejected simply for not including code, unless this is central to the contribution (e.g., for a new open-source benchmark).
- The instructions should contain the exact command and environment needed to run to reproduce the results. See the NeurIPS code and data submission guidelines (<https://nips.cc/public/guides/CodeSubmissionPolicy>) for more details.
- The authors should provide instructions on data access and preparation, including how to access the raw data, preprocessed data, intermediate data, and generated data, etc.
- The authors should provide scripts to reproduce all experimental results for the new proposed method and baselines. If only a subset of experiments are reproducible, they should state which ones are omitted from the script and why.
- At submission time, to preserve anonymity, the authors should release anonymized versions (if applicable).
- Providing as much information as possible in supplemental material (appended to the paper) is recommended, but including URLs to data and code is permitted.

vi. **Experimental setting/details**

Question: Does the paper specify all the training and test details (e.g., data splits, hyper-parameters, how they were chosen, type of optimizer, etc.) necessary to understand the results?

Answer: [Yes]

Justification: Section 4.1 of the main paper and Appendix G provide comprehensive details necessary to reproduce our main experimental results. Additionally, we will release our code and pretrained models to support future research and facilitate further exploration of our approach.

Guidelines:

- The answer NA means that the paper does not include experiments.
- The experimental setting should be presented in the core of the paper to a level of detail that is necessary to appreciate the results and make sense of them.
- The full details can be provided either with the code, in appendix, or as supplemental material.

vii. **Experiment statistical significance**

Question: Does the paper report error bars suitably and correctly defined or other appropriate information about the statistical significance of the experiments?

Answer: [Yes]

Justification: Results are averaged over three independent runs with different random seeds for robustness.

Guidelines:

- The answer NA means that the paper does not include experiments.

- The authors should answer "Yes" if the results are accompanied by error bars, confidence intervals, or statistical significance tests, at least for the experiments that support the main claims of the paper.
- The factors of variability that the error bars are capturing should be clearly stated (for example, train/test split, initialization, random drawing of some parameter, or overall run with given experimental conditions).
- The method for calculating the error bars should be explained (closed form formula, call to a library function, bootstrap, etc.)
- The assumptions made should be given (e.g., Normally distributed errors).
- It should be clear whether the error bar is the standard deviation or the standard error of the mean.
- It is OK to report 1-sigma error bars, but one should state it. The authors should preferably report a 2-sigma error bar than state that they have a 96% CI, if the hypothesis of Normality of errors is not verified.
- For asymmetric distributions, the authors should be careful not to show in tables or figures symmetric error bars that would yield results that are out of range (e.g. negative error rates).
- If error bars are reported in tables or plots, The authors should explain in the text how they were calculated and reference the corresponding figures or tables in the text.

viii. **Experiments compute resources**

Question: For each experiment, does the paper provide sufficient information on the computer resources (type of compute workers, memory, time of execution) needed to reproduce the experiments?

Answer: [Yes]

Justification: Section 4.1 of the main paper and Appendix G provide comprehensive details necessary to reproduce our main experimental results. Additionally, we will release our code and pretrained models to support future research and facilitate further exploration of our approach.

Guidelines:

- The answer NA means that the paper does not include experiments.
- The paper should indicate the type of compute workers CPU or GPU, internal cluster, or cloud provider, including relevant memory and storage.
- The paper should provide the amount of compute required for each of the individual experimental runs as well as estimate the total compute.
- The paper should disclose whether the full research project required more compute than the experiments reported in the paper (e.g., preliminary or failed experiments that didn't make it into the paper).

ix. **Code of ethics**

Question: Does the research conducted in the paper conform, in every respect, with the NeurIPS Code of Ethics <https://neurips.cc/public/EthicsGuidelines?>

Answer: [Yes]

Justification: The research conducted in the paper conform, in every respect, with the NeurIPS Code of Ethics.

Guidelines:

- The answer NA means that the authors have not reviewed the NeurIPS Code of Ethics.
- If the authors answer No, they should explain the special circumstances that require a deviation from the Code of Ethics.
- The authors should make sure to preserve anonymity (e.g., if there is a special consideration due to laws or regulations in their jurisdiction).

x. **Broader impacts**

Question: Does the paper discuss both potential positive societal impacts and negative societal impacts of the work performed?

Answer: [Yes]

Justification: Appendix J discusses both the potential positive and negative societal impacts of this work.

Guidelines:

- The answer NA means that there is no societal impact of the work performed.
- If the authors answer NA or No, they should explain why their work has no societal impact or why the paper does not address societal impact.
- Examples of negative societal impacts include potential malicious or unintended uses (e.g., disinformation, generating fake profiles, surveillance), fairness considerations (e.g., deployment of technologies that could make decisions that unfairly impact specific groups), privacy considerations, and security considerations.
- The conference expects that many papers will be foundational research and not tied to particular applications, let alone deployments. However, if there is a direct path to any negative applications, the authors should point it out. For example, it is legitimate to point out that an improvement in the quality of generative models could be used to generate deepfakes for disinformation. On the other hand, it is not needed to point out that a generic algorithm for optimizing neural networks could enable people to train models that generate Deepfakes faster.
- The authors should consider possible harms that could arise when the technology is being used as intended and functioning correctly, harms that could arise when the technology is being used as intended but gives incorrect results, and harms following from (intentional or unintentional) misuse of the technology.
- If there are negative societal impacts, the authors could also discuss possible mitigation strategies (e.g., gated release of models, providing defenses in addition to attacks, mechanisms for monitoring misuse, mechanisms to monitor how a system learns from feedback over time, improving the efficiency and accessibility of ML).

xi. Safeguards

Question: Does the paper describe safeguards that have been put in place for responsible release of data or models that have a high risk for misuse (e.g., pretrained language models, image generators, or scraped datasets)?

Answer: [NA]

Justification: To the best of our knowledge, this work poses no foreseeable risks of misuse, such as those associated with pretrained language models, generative image systems, or the use of scraped datasets.

Guidelines:

- The answer NA means that the paper poses no such risks.
- Released models that have a high risk for misuse or dual-use should be released with necessary safeguards to allow for controlled use of the model, for example by requiring that users adhere to usage guidelines or restrictions to access the model or implementing safety filters.
- Datasets that have been scraped from the Internet could pose safety risks. The authors should describe how they avoided releasing unsafe images.
- We recognize that providing effective safeguards is challenging, and many papers do not require this, but we encourage authors to take this into account and make a best faith effort.

xii. Licenses for existing assets

Question: Are the creators or original owners of assets (e.g., code, data, models), used in the paper, properly credited and are the license and terms of use explicitly mentioned and properly respected?

Answer: [Yes]

Justification: The original creators or owners of all assets used in this paper (e.g., code, data, models) are properly credited, and the associated licenses and terms of use are explicitly acknowledged and fully respected.

Guidelines:

- The answer NA means that the paper does not use existing assets.
- The authors should cite the original paper that produced the code package or dataset.
- The authors should state which version of the asset is used and, if possible, include a URL.
- The name of the license (e.g., CC-BY 4.0) should be included for each asset.
- For scraped data from a particular source (e.g., website), the copyright and terms of service of that source should be provided.
- If assets are released, the license, copyright information, and terms of use in the package should be provided. For popular datasets, paperswithcode.com/datasets has curated licenses for some datasets. Their licensing guide can help determine the license of a dataset.
- For existing datasets that are re-packaged, both the original license and the license of the derived asset (if it has changed) should be provided.
- If this information is not available online, the authors are encouraged to reach out to the asset's creators.

xiii. **New assets**

Question: Are new assets introduced in the paper well documented and is the documentation provided alongside the assets?

Answer: [Yes]

Justification: Section 4.1 of the main paper and Appendix G provide comprehensive details necessary to reproduce our main experimental results. Additionally, we will release our code and pretrained models to support future research and facilitate further exploration of our approach. We will use structured templates on GitHub, which will include details on training, licensing, limitations, and more.

Guidelines:

- The answer NA means that the paper does not release new assets.
- Researchers should communicate the details of the dataset/code/model as part of their submissions via structured templates. This includes details about training, license, limitations, etc.
- The paper should discuss whether and how consent was obtained from people whose asset is used.
- At submission time, remember to anonymize your assets (if applicable). You can either create an anonymized URL or include an anonymized zip file.

xiv. **Crowdsourcing and research with human subjects**

Question: For crowdsourcing experiments and research with human subjects, does the paper include the full text of instructions given to participants and screenshots, if applicable, as well as details about compensation (if any)?

Answer: [NA]

Justification: This paper does not involve crowdsourcing nor research with human subjects.

Guidelines:

- The answer NA means that the paper does not involve crowdsourcing nor research with human subjects.
- Including this information in the supplemental material is fine, but if the main contribution of the paper involves human subjects, then as much detail as possible should be included in the main paper.
- According to the NeurIPS Code of Ethics, workers involved in data collection, curation, or other labor should be paid at least the minimum wage in the country of the data collector.

xv. **Institutional review board (IRB) approvals or equivalent for research with human subjects**

Question: Does the paper describe potential risks incurred by study participants, whether such risks were disclosed to the subjects, and whether Institutional Review Board (IRB) approvals (or an equivalent approval/review based on the requirements of your country or institution) were obtained?

Answer: [NA]

Justification: This paper does not involve crowdsourcing nor research with human subjects.

Guidelines:

- The answer NA means that the paper does not involve crowdsourcing nor research with human subjects.
- Depending on the country in which research is conducted, IRB approval (or equivalent) may be required for any human subjects research. If you obtained IRB approval, you should clearly state this in the paper.
- We recognize that the procedures for this may vary significantly between institutions and locations, and we expect authors to adhere to the NeurIPS Code of Ethics and the guidelines for their institution.
- For initial submissions, do not include any information that would break anonymity (if applicable), such as the institution conducting the review.

xvi. **Declaration of LLM usage**

Question: Does the paper describe the usage of LLMs if it is an important, original, or non-standard component of the core methods in this research? Note that if the LLM is used only for writing, editing, or formatting purposes and does not impact the core methodology, scientific rigorosity, or originality of the research, declaration is not required.

Answer: [NA]

Justification: The core methodology developed in this research does not involve LLMs or any important, original, or non-standard components related to them.

Guidelines:

- The answer NA means that the core method development in this research does not involve LLMs as any important, original, or non-standard components.
- Please refer to our LLM policy (<https://neurips.cc/Conferences/2025/LLM>) for what should or should not be described.

A Relation to Existing Paradigms

Below, we situate GCR within these paradigms, highlighting its unique contributions and distinctions.

Graph-based learning and relational alignment. Graph-based methods are widely used to model relational structures in classification [56, 92, 127] and semi-supervised learning [96, 11, 82], often through pre-constructed graphs [109, 125] or memory banks [68]. Traditional approaches use graph Laplacian regularization [80, 4] or GNN-based message passing [13, 40] to encourage feature alignment. While powerful, these methods require explicit graph definitions or heavy architectural components like GNNs and GATs [61, 102].

GCR diverges fundamentally from these strategies:

- i. **On-the-fly graph construction.** Instead of relying on static or memory-driven graphs [36, 56, 76], GCR builds internal graphs dynamically during training, using model-generated predictions and feature embeddings.
- ii. **Regularization, not transformation.** Unlike GNNs that propagate features [89, 10, 85], GCR purely regularizes the relational structure of features to enforce alignment with class-aware prediction similarity.
- iii. **Parameter-free alignment.** GCR operates without additional parameters for graph construction, using only the inherent feature and prediction relationships for alignment.

This design enables GCR to maintain the benefits of relational modeling while being model-agnostic and computationally efficient, extending graph-based learning into deeper, more flexible architectures. Furthermore, GCR enhances generalization by implicitly smoothing decision boundaries through its consistency-driven alignment, even in high-dimensional feature spaces.

Contrastive learning and semantic consistency. Contrastive methods [60, 118, 45] pull together positive pairs and push apart negatives, often using data augmentation [99, 107] and hard negative mining for improved class separation [14, 60]. However, these methods are sensitive to sampling strategies [116, 19] and require margin tuning for stability [34].

GCR introduces a contrastive mechanism that is *global and implicit*:

- i. **Global relational alignment.** Rather than pairwise contrasts [17], GCR aligns the entire feature graph and prediction graph, capturing holistic relationships across the batch.
- ii. **Self-supervised by prediction.** The semantic graph is constructed directly from model predictions, obviating the need for manual sampling or augmentation strategies [72, 19].
- iii. **Semantic geometric regularization.** GCR enforces global coherence between semantic and geometric structures, extending beyond local distances to full-batch relational consistency.

This implicit contrastive mechanism ensures stable alignment of semantic structures without the pitfalls of traditional contrastive learning, contributing to stronger robustness against noisy samples and domain shifts.

Structural regularization and manifold learning. Traditional regularizers like center loss [86, 84] and triplet loss [24, 119, 29] enforce feature compactness or inter-class margins, while graph Laplacian regularization [80, 4] smooths label propagation over fixed data graphs [7, 130]. However, these approaches [78, 98, 94] are limited by predefined graphs or local constraints.

GCR generalizes structural regularization with three core innovations:

- i. **Dynamic graph construction.** GCR constructs feature graphs and prediction graphs on-the-fly during each training iteration, adapting to the model’s evolving internal representations.
- ii. **Cross-space alignment.** Unlike classical manifold regularization, which only smooths feature relationships, GCR aligns semantic (prediction-based) and geometric (feature-based) graphs, ensuring that class-consistent features are also prediction-consistent.
- iii. **Masked supervision.** GCR enforces class-aware masking during alignment, preventing smoothing across semantic boundaries and refining intra-class structure.

This structural regularization not only preserves semantic coherence but also improves robust generalization by dynamically capturing the evolving feature manifold of the network.

Self-conditioning and geometric representation learning. Self-conditioning mechanisms [58] like prompting typically rely on external tokens or model outputs to influence learning trajectories [67, 21].

GCR extends this paradigm internally by using the model’s own prediction graph as a self-generated scaffold:

- i. **Relational prompting.** Unlike discrete prompts [12, 83, 65], GCR uses prediction-induced graphs to continuously adjust feature relationships according to class structure.
- ii. **Semantic geometry emergence.** Geometric deep learning traditionally imposes structural priors [87]; GCR allows semantic geometry to emerge organically through predictive alignment [8, 33].
- iii. **Continuous, implicit supervision.** This prediction-based regularization evolves with the model, providing ongoing, context-aware structure during training.

GCR thus bridges self-conditioning with geometric learning, establishing semantic-aware representation that dynamically evolves with the model’s understanding of its own predictions.

GCR’s design is rooted in manifold alignment theory and smoothness regularization: by enforcing consistency between feature similarity and prediction similarity, it effectively smooths decision boundaries in feature space, enhancing generalization across unseen domains. This principle is akin to cluster assumption in semi-supervised learning, where similar samples are encouraged to share the same label.

B Graph Consistency as Self-Prompting

We interpret GCR as a form of internal *prompting*, where the model dynamically generates its own prompting signal from its predictions to guide the learning of intermediate features. This contrasts with traditional prompting approaches, which typically rely on external tokens or instructions to influence the model’s behavior.

Key characteristics of GCR as self-prompting include:

- i. **Internal.** The prompting signal originates entirely from the model’s own predictions, eliminating the need for external input.
- ii. **Structural.** The alignment operates over pairwise relationships within the feature space, focusing on how different features relate to one another rather than conditioning on individual samples.
- iii. **Semantic.** The graph structure is inherently class-aware, encouraging the network to adjust its feature representations to align with meaningful semantic boundaries between classes.

In this framework, the prediction graph acts as a learned, self-supervised attention template that recursively guides the refinement of feature representations in earlier layers. This novel approach paves the way for self-conditioning in neural networks, where the model’s own predictions continuously inform and improve its internal feature learning process.

C Motivation

Deep neural networks have excelled at learning complex, hierarchical feature representations. Typically, early layers capture low-level visual cues such as edges, textures, and basic shapes, which are often sensitive to noise and not specific to the task. In contrast, deeper layers develop high-level features that reflect more semantic, task-relevant information. However, despite achieving clear class separation in the final prediction space, intermediate feature spaces can still exhibit significant inter-class overlap. This overlap weakens both the generalization ability and the discriminative power of the model.

Furthermore, during training, the parameter search space remains vast because supervision is driven only by class labels, without using any explicit relational structure among samples. This lack of structure-aware guidance limits the model’s ability to organize its feature space meaningfully.

We propose that the model’s own predictions contain rich semantic information that can serve as a self-supervisory signal. Specifically, the pairwise similarities among prediction logits encode a high-level semantic topology that reflects class affinities. By aligning intermediate feature representations with this prediction-derived structure, we encourage the network to learn representations that are geometrically consistent with semantic class boundaries.

Our approach is guided by the following insights:

- i. **Reduce noisy inter-class affinities.** By aligning feature graphs with prediction graphs, we minimize the risk of inter-class features being too similar, thereby reducing class overlap in the feature space.
- ii. **Enhance intra-class cohesion.** Encouraging feature consistency within each class ensures that the network’s representations exhibit stronger intra-class similarity.
- iii. **Align learning dynamics with semantic intent.** Through the introduction of prediction-guided alignment, we direct the network’s learning trajectory to reflect global semantic structures, improving generalization and interpretability.

Thus, we treat the prediction graph as an implicit *structural prompt* that guides the network’s learning. This contrasts with traditional methods, where supervision typically focuses on final output layers. Our approach integrates structural coherence directly into the intermediate layers of the network, creating a rich, semantic-aware feature representation pipeline.

D Theoretical Insights

We analyze GCR from a theoretical perspective, grounding it in the manifold hypothesis, spectral graph theory, and statistical learning theory.

D.1 Manifold Smoothness and Semantic Cluster Regularization

Definition 1 (Data manifold hypothesis). *Let $\mathcal{X} \subset \mathbb{R}^d$ be the input space. The data manifold hypothesis posits that real-world data points $\{x_i\}_{i=1}^n$ lie on or near a smooth, compact m -dimensional Riemannian manifold $\mathcal{M} \subset \mathbb{R}^d$, where $m \ll d$.*

Definition 2 (Feature relational graph). *Let $f^{(l)}(x_i) \in \mathbb{R}^p$ denote the feature representation of sample x_i at layer l . The feature similarity matrix $\mathbf{F}^{(l)} \in \mathbb{R}^{n \times n}$ as feature relational graph is defined by:*

$$\mathbf{F}_{ij}^{(l)} := \text{ReLU} \left(\cos \left(\mathbf{x}_i^{(l)}, \mathbf{x}_j^{(l)} \right) \right) = \text{ReLU} \left(\frac{\langle \mathbf{x}_i^{(l)}, \mathbf{x}_j^{(l)} \rangle}{\|\mathbf{x}_i^{(l)}\| \|\mathbf{x}_j^{(l)}\|} \right).$$

Definition 3 (Masked prediction relational graph). *Let \mathbf{z}_i be the pre-softmax prediction logits for sample x_i , and define $\mathbf{s}_i := \text{softmax}(\mathbf{z}_i)$. The semantic similarity between predictions is computed as:*

$$\mathbf{S}_{ij} := \text{ReLU} \left(\cos \left(\mathbf{s}_i, \mathbf{s}_j \right) \right).$$

Let $\mathbf{M}_{ij} := \mathbb{1}[y_i = y_j]$ be a binary mask indicating whether two samples belong to the same class. The masked prediction relational graph is then:

$$\mathbf{P}_{ij} := \mathbf{M}_{ij} \odot \mathbf{S}_{ij}.$$

Proposition 3 (Manifold smoothness regularization). *Minimizing the alignment loss $\|\mathbf{F}^{(l)} - \mathbf{P}\|_F^2$ enforces local smoothness on the feature manifold. Specifically, if $\mathbf{P}_{ij} > 0$, then*

$$\|\mathbf{x}_i^{(l)} - \mathbf{x}_j^{(l)}\|^2 = 2 - 2 \cos \left(\mathbf{x}_i^{(l)}, \mathbf{x}_j^{(l)} \right) \rightarrow 0.$$

Proof. For any i, j such that $\mathbf{P}_{ij} > 0$, the squared Frobenius loss penalizes the discrepancy between $\mathbf{F}_{ij}^{(l)}$ and \mathbf{P}_{ij} . Since $\mathbf{F}_{ij}^{(l)}$ is a monotonic decreasing function of $\|\mathbf{x}_i^{(l)} - \mathbf{x}_j^{(l)}\|^2$, minimizing this loss implies that $\mathbf{x}_i^{(l)}$ and $\mathbf{x}_j^{(l)}$ must be close in feature space ($y_i = y_j$). Therefore, GCR promotes smoothness by aligning local geometry with semantic similarity. \square

Definition 4 (Cluster assumption). *The cluster assumption asserts that samples from the same class form tight, compact clusters in representation space. That is, for $y_i = y_j$, we expect $\|\mathbf{x}_i^{(l)} - \mathbf{x}_j^{(l)}\|^2$ to be small, while for $y_i \neq y_j$, the distance should be large.*

Proposition 4 (Semantic cluster regularization). *Minimizing the GCR loss:*

$$\mathcal{L}_{GCR} = \sum_l \left\| \mathbf{F}^{(l)} - \mathbf{P} \right\|_F^2,$$

promotes intra-class compactness and inter-class separation in the feature space, thereby aligning learned features with semantic class structure.

Proof. When $y_i = y_j$, the mask $\mathbf{M}_{ij} = 1$, so \mathbf{P}_{ij} is proportional to the prediction similarity \mathbf{S}_{ij} . A large \mathbf{P}_{ij} enforces a corresponding increase in $\mathbf{F}_{ij}^{(l)}$, which implies a smaller angle and distance between $\mathbf{x}_i^{(l)}$ and $\mathbf{x}_j^{(l)}$. Conversely, for $y_i \neq y_j$, $\mathbf{P}_{ij} = 0$, and there is no incentive to keep $\mathbf{x}_i^{(l)}$ and $\mathbf{x}_j^{(l)}$ close. This results in greater inter-class separation and aligns the learned representation with class structure. \square

D.2 Connection to Graph Laplacian Regularization

From cosine similarity to Graph Laplacians. GCR aligns feature similarity graphs $\mathbf{F}^{(l)}$ with semantic prediction graphs \mathbf{P} at each selected layer l . Both graphs are constructed using ReLU-activated cosine similarity, forming symmetric, non-negative affinity matrices:

$$\begin{aligned} \mathbf{F}_{ij}^{(l)} &= \text{ReLU}(\cos(\mathbf{x}_i^{(l)}, \mathbf{x}_j^{(l)})), \\ \mathbf{P}_{ij} &= \mathbf{M}_{ij} \odot \text{ReLU}(\cos(\mathbf{s}_i, \mathbf{s}_j)), \end{aligned}$$

where \mathbf{s}_i are softmax-normalized logits. Although these graphs do not use an RBF kernel, they still induce a graph structure with meaningful edge weights and comparable degree distributions across layers. Since the GCL operates on strictly upper-triangular entries, the resulting Laplacians remain symmetric and well-defined.

Definition 5 (Graph Laplacian). *Given an affinity matrix $\mathbf{A} \in \mathbb{R}^{n \times n}$ (e.g., $\mathbf{F}^{(l)}$ or \mathbf{P}), the unnormalized graph Laplacian is defined as:*

$$\mathbf{L} = \mathbf{D} - \mathbf{A}, \quad \text{where } \mathbf{D}_{ii} = \sum_j \mathbf{A}_{ij}.$$

Semantic alignment via spectral consistency. While the classical result by Belkin and Niyogi [6] connects RBF-based graph Laplacians to the Laplace-Beltrami operator on manifolds, our cosine-based affinity still permits an analogous interpretation in terms of structural smoothness. In particular, minimizing alignment loss between $\mathbf{F}^{(l)}$ and \mathbf{P} induces convergence between their associated Laplacians \mathbf{L}_F and \mathbf{L}_P .

Proposition 5 (Spectral regularization via Laplacian alignment). *If $\|\mathbf{F}^{(l)} - \mathbf{P}\|_F^2$ is small, then the spectral properties of \mathbf{L}_F and \mathbf{L}_P are closely aligned. Minimizing GCR encourages*

$$\text{Tr}(\mathbf{x}^{(l)\top} \mathbf{L}_F \mathbf{x}^{(l)}) \approx \text{Tr}(\mathbf{x}^{(l)\top} \mathbf{L}_P \mathbf{x}^{(l)}),$$

thus regularizing features to follow both local geometric and global semantic structure.

Sketch. For symmetric matrices with matching degrees, $\mathbf{F}^{(l)} \approx \mathbf{P} \Rightarrow \mathbf{L}_F \approx \mathbf{L}_P$. The quadratic form $\text{Tr}(\mathbf{x}^\top \mathbf{L} \mathbf{x})$ measures smoothness over the graph. Alignment thus enforces semantic-aware smoothness. \square

D.3 Generalization Bound under Structural Alignment

We now provide a detailed theoretical analysis of how GCR contributes to improved generalization. Our goal is to show that by enforcing alignment between the feature graph and the semantic prediction graph, GCR effectively restricts the function class to smoother, semantically consistent representations, leading to a reduced Rademacher complexity.

Definition 6 (Structural alignment loss). Let $f^{(l)} : \mathcal{X} \rightarrow \mathbb{R}^d$ be the feature mapping at layer l . We define the GCR structural loss at layer l as:

$$\mathcal{L}_{GCR}^{(l)} := \frac{1}{n^2} \sum_{i,j} \left(\mathbf{F}_{ij}^{(l)} - \mathbf{P}_{ij} \right)^2.$$

Definition 7 (Structurally constrained function class). Let \mathcal{F}_L be the class of functions $f^{(l)}$ such that $\|f^{(l)}(x)\|_2 \leq B$ for all $x \in \mathcal{X}$ and all l . Then the GCR-constrained function class is:

$$\mathcal{F}_\epsilon := \left\{ f^{(l)} \in \mathcal{F}_L \mid \mathcal{L}_{GCR}^{(l)} \leq \epsilon \right\}.$$

This class enforces that features not only have bounded norm but also align structurally with the prediction graph \mathbf{P} in the sense of Frobenius proximity.

Theorem 3 (Generalization bound under GCR). Let $\ell(f(x), y)$ be a γ -Lipschitz loss function (e.g., cross-entropy), and suppose $f \in \mathcal{F}_\epsilon$. Then with probability at least $1 - \delta$, the generalization error is bounded as:

$$\mathbb{E}_{(x,y) \sim \mathcal{D}}[\ell(f(x), y)] \leq \frac{1}{n} \sum_{i=1}^n \ell(f(x_i), y_i) + \frac{4\gamma B \sqrt{\epsilon}}{n} + \mathcal{O}\left(\sqrt{\frac{\log(1/\delta)}{n}}\right).$$

Proof. Let $\mathfrak{R}_n(\mathcal{F}_\epsilon)$ denote the empirical Rademacher complexity of \mathcal{F}_ϵ :

$$\mathfrak{R}_n(\mathcal{F}_\epsilon) := \mathbb{E}_\sigma \left[\sup_{f \in \mathcal{F}_\epsilon} \frac{1}{n} \sum_{i=1}^n \sigma_i f(x_i) \right],$$

where σ_i are i.i.d. Rademacher random variables taking values ± 1 with equal probability.

We apply the contraction lemma, which states that if ℓ is γ -Lipschitz, then:

$$\mathfrak{R}_n(\ell \circ \mathcal{F}_\epsilon) \leq \gamma \cdot \mathfrak{R}_n(\mathcal{F}_\epsilon).$$

Now we aim to bound $\mathfrak{R}_n(\mathcal{F}_\epsilon)$. Since each function $f \in \mathcal{F}_\epsilon$ maps $x_i \mapsto \mathbf{x}_i^{(l)} \in \mathbb{R}^d$ with $\|\mathbf{x}_i^{(l)}\|_2 \leq B$ and whose pairwise ReLU-cosine similarities are constrained to align with \mathbf{P}_{ij} , the variability of outputs is tightly controlled. Specifically, we define:

$$\mathbf{F}_{ij}^{(l)} = \text{ReLU}(\langle \mathbf{x}_i^{(l)}, \mathbf{x}_j^{(l)} \rangle), \quad \text{and} \quad \sum_{i,j} (\mathbf{F}_{ij}^{(l)} - \mathbf{P}_{ij})^2 \leq n^2 \epsilon.$$

Note that for normalized vectors, $\langle \mathbf{x}_i^{(l)}, \mathbf{x}_j^{(l)} \rangle = \cos \theta_{ij}$, and the ReLU ensures non-negativity. The loss penalizes angles between feature vectors that deviate from their semantically guided prediction-based affinity.

Let us now relate this to a bound on the Rademacher complexity. We use the following result adapted from Bartlett and Mendelson (2002): for any bounded function $f(x) \in \mathbb{R}^d$ with $\|f(x)\|_2 \leq B$, the Rademacher complexity is bounded by:

$$\mathfrak{R}_n(\mathcal{F}_L) \leq \frac{B}{n} \mathbb{E}_\sigma \left[\left\| \sum_{i=1}^n \sigma_i \right\| \right] = \frac{B}{\sqrt{n}}.$$

However, for \mathcal{F}_ϵ , we have a stronger constraint: the features cannot vary arbitrarily due to the structural alignment requirement. In particular, for small ϵ , all $\mathbf{x}_i^{(l)}$ are geometrically organized to maintain high similarity (angle $\rightarrow 0$) when \mathbf{P}_{ij} is high and to be less constrained otherwise.

Hence, the variance in $f(x)$ is suppressed in directions orthogonal to semantic affinity, shrinking the function class. From this, one can derive:

$$\mathfrak{R}_n(\mathcal{F}_\epsilon) \leq \frac{2B\sqrt{\epsilon}}{n},$$

where the $\sqrt{\epsilon}$ factor reflects the deviation from perfect structural alignment.

Substituting into the standard generalization bound yields:

$$\mathbb{E}[\ell(f(x), y)] \leq \frac{1}{n} \sum_{i=1}^n \ell(f(x_i), y_i) + \frac{4\gamma B \sqrt{\epsilon}}{n} + \mathcal{O}\left(\sqrt{\frac{\log(1/\delta)}{n}}\right).$$

□

Remark 3. *This bound demonstrates that GCR effectively reduces the hypothesis complexity by enforcing a semantic structure on the learned representations. As the structural loss ϵ decreases, the model class is increasingly constrained to semantically faithful functions, thereby improving generalization on unseen data.*

GCR aligns feature similarity graphs with semantically meaningful prediction graphs, enforcing both geometric and semantic smoothness. Our analysis shows GCR promotes manifold alignment, Laplacian smoothness, semantic clustering, and provably better generalization.

E Proof for Theoretical Analysis of GCR

We provide a theoretical analysis of GCR, connecting its empirical design to foundational concepts in statistical learning theory and spectral graph theory. Specifically, we show that minimizing the GCR loss: (i) Reduces the effective capacity of the hypothesis class via covering number bounds and Dudley’s entropy integral. (ii) Promotes spectral consistency between learned features and semantically meaningful prediction graphs via normalized Laplacians. (iii) Can be interpreted as a PAC-Bayesian regularizer that imposes a structural prior on function space.

E.1 Generalization via Covering Numbers

Let \mathcal{F}_L be the class of functions $f^{(l)} : \mathcal{X} \rightarrow \mathbb{R}^d$ representing the layer- l embeddings. B is a constant upper bound on the ℓ_2 norm of the feature representation $f^{(l)}(x) \in \mathbb{R}^d$ at layer l . That is,

$$\|f^{(l)}(x)\|_2 = \sqrt{\sum_{i=1}^d \left(f_i^{(l)}(x)\right)^2} \leq B, \text{ for all } x \in \mathcal{X}.$$

This constraint is standard in learning theory to control the size of the hypothesis space. In practice, especially under L2 normalization used in our method, we often have $B = 1$. We then define a structurally-constrained hypothesis class:

$$\mathcal{F}_\epsilon := \left\{ f \in \mathcal{F}_L : \mathcal{L}_{\text{GCR}}^{(l)} := \|\text{triu}(\mathbf{F}^{(l)}) - \text{triu}(\mathbf{P})\|_F^2 \leq \epsilon \right\}. \quad (16)$$

This class enforces graph alignment between learned features and the masked prediction graph \mathbf{P} , which reflects intra-class similarity.

Theorem 4 (Generalization via Dudley’s entropy integral). *Let $\ell(f(x), y)$ be a γ -Lipschitz loss function (e.g., cross-entropy), and let \mathcal{F}_L be the class of functions at layer l such that each function $f^{(l)}$ satisfies the ℓ_2 -bounded constraint $\|f^{(l)}(x)\|_2 \leq B$. Suppose $\mathcal{F}_\epsilon \subseteq \mathcal{F}_L$ is the subset of functions that are additionally constrained by the GCR alignment loss:*

$$\mathcal{L}_{\text{GCR}}^{(l)} = \frac{1}{n^2} \sum_{i,j=1}^n (\text{ReLU}(\langle \mathbf{x}_i, \mathbf{x}_j \rangle) - \mathbf{P}_{ij})^2 \leq \epsilon, \quad (17)$$

where $\mathbf{x}_i = \frac{f^{(l)}(x_i)}{\|f^{(l)}(x_i)\|_2}$ are the normalized feature vectors for each data point x_i in the dataset, and \mathbf{P}_{ij} is the target alignment between the feature vectors \mathbf{x}_i and \mathbf{x}_j . The GCR loss enforces that the angular distances between the feature vectors are small, meaning that the vectors are close to each other in the Euclidean space.

If \mathcal{F}_ϵ admits a covering number bound:

$$\mathcal{N}(\mathcal{F}_\epsilon, \|\cdot\|_2, \alpha) \leq \left(\frac{C}{\alpha}\right)^d, \quad (18)$$

where $\mathcal{N}(\mathcal{F}_\epsilon, \|\cdot\|_2, \alpha)$ is the covering number of \mathcal{F}_ϵ with respect to the ℓ_2 norm, then the expected loss of a function $f \in \mathcal{F}_\epsilon$ is bounded with high probability by:

$$\mathbb{E}_{(x,y) \sim \mathcal{D}}[\ell(f(x), y)] \leq \frac{1}{n} \sum_{i=1}^n \ell(f(x_i), y_i) + \frac{12\gamma}{\sqrt{n}} \int_0^B \sqrt{d \log \left(\frac{C}{\alpha} \right)} d\alpha, \quad (19)$$

where $B = O(\sqrt{\epsilon})$ is the effective radius of the function class \mathcal{F}_ϵ under the GCR constraint, and the second term represents the generalization error, which is controlled by the complexity of the function class.

Proof Sketch. We outline the key steps:

Step 1: Rademacher complexity controls generalization. Let $\mathfrak{R}_n(\mathcal{F}_\epsilon)$ denote the empirical Rademacher complexity of the constrained class. Since the loss function ℓ is γ -Lipschitz, the composition inequality gives:

$$\mathfrak{R}_n(\ell \circ \mathcal{F}_\epsilon) \leq \gamma \cdot \mathfrak{R}_n(\mathcal{F}_\epsilon).$$

Step 2: Dudley's entropy integral. We now bound $\mathfrak{R}_n(\mathcal{F}_\epsilon)$ using Dudley's entropy integral:

$$\mathfrak{R}_n(\mathcal{F}_\epsilon) \leq \frac{12}{\sqrt{n}} \int_0^{\text{diam}(\mathcal{F}_\epsilon)} \sqrt{\log \mathcal{N}(\mathcal{F}_\epsilon, \|\cdot\|_2, \alpha)} d\alpha,$$

where $\text{diam}(\mathcal{F}_\epsilon)$ refers to the diameter of the set \mathcal{F}_ϵ , *i.e.*, the largest possible distance between any two points in \mathcal{F}_ϵ in Euclidean space.

Step 3: Diameter bound under GCR. Under the GCR constraint, $\mathbf{F}_{ij}^{(l)} = \text{ReLU}(\langle \mathbf{x}_i, \mathbf{x}_j \rangle)$ is close to \mathbf{P}_{ij} . Since both \mathbf{x}_i and \mathbf{x}_j are unit-normalized vectors, this implies that the angular distances between them are bounded. Let $\langle \mathbf{x}_i, \mathbf{x}_j \rangle \geq \tau$ for pairs where $\mathbf{P}_{ij} > 0$. This cosine similarity constraint restricts pairwise angles to lie within a narrow cone. Therefore, the effective diameter of \mathcal{F}_ϵ in Euclidean space is:

$$\|\mathbf{x}_i - \mathbf{x}_j\|_2 \leq \sqrt{2 - 2 \cos \theta} \approx O(\sqrt{\epsilon}),$$

where θ is the angle between \mathbf{x}_i and \mathbf{x}_j . Thus, we set $B = O(\sqrt{\epsilon})$.

Step 4: Plug in covering number. Using the assumed covering number bound $\mathcal{N}(\alpha) \leq (C/\alpha)^d$, we have:

$$\log \mathcal{N}(\mathcal{F}_\epsilon, \|\cdot\|_2, \alpha) \leq d \log(C/\alpha).$$

Step 5: Final bound. Substitute into Dudley's integral:

$$\mathfrak{R}_n(\mathcal{F}_\epsilon) \leq \frac{12}{\sqrt{n}} \int_0^B \sqrt{d \log \left(\frac{C}{\alpha} \right)} d\alpha,$$

and apply the composition inequality to yield the desired result. \square

Remark 4. This result shows that GCR reduces generalization error by shrinking the effective complexity of the function class. By aligning relational structure, GCR implicitly contracts the hypothesis space, leading to improved generalization.

E.2 Spectral Alignment via Normalized Laplacians

Let \mathbf{F} and \mathbf{P} be symmetric affinity matrices derived from feature embeddings and masked predictions, respectively. Their associated normalized graph Laplacians are defined as:

$$\mathcal{L}_{\mathbf{F}} := \mathbf{I} - \mathbf{D}_{\mathbf{F}}^{-1/2} \mathbf{F} \mathbf{D}_{\mathbf{F}}^{-1/2}, \quad \mathcal{L}_{\mathbf{P}} := \mathbf{I} - \mathbf{D}_{\mathbf{P}}^{-1/2} \mathbf{P} \mathbf{D}_{\mathbf{P}}^{-1/2},$$

where $\mathbf{D}_{\mathbf{F}}$ and $\mathbf{D}_{\mathbf{P}}$ are the degree matrices corresponding to \mathbf{F} and \mathbf{P} , *i.e.*, $(\mathbf{D}_{\mathbf{F}})_{ii} = \sum_j \mathbf{F}_{ij}$ and similarly for $\mathbf{D}_{\mathbf{P}}$.

Proposition 6 (Spectral Alignment). Let \mathbf{F} and \mathbf{P} be symmetric matrices such that

$$\|\mathbf{F} - \mathbf{P}\|_F \leq \epsilon, \quad \|\mathbf{D}_{\mathbf{F}} - \mathbf{D}_{\mathbf{P}}\| \leq \delta.$$

Then, there exists a constant $C > 0$ depending on spectral properties of the graphs (*e.g.*, sparsity, minimum degree), such that

$$\|\mathcal{L}_{\mathbf{F}} - \mathcal{L}_{\mathbf{P}}\|_F \leq C(\epsilon + \delta). \quad (20)$$

Proof Sketch. We aim to bound the difference between the normalized Laplacians $\mathcal{L}_{\mathbf{F}}$ and $\mathcal{L}_{\mathbf{P}}$ in Frobenius norm. We begin by expanding the difference:

$$\|\mathcal{L}_{\mathbf{F}} - \mathcal{L}_{\mathbf{P}}\|_F = \left\| \left(\mathbf{I} - \mathbf{D}_{\mathbf{F}}^{-1/2} \mathbf{F} \mathbf{D}_{\mathbf{F}}^{-1/2} \right) - \left(\mathbf{I} - \mathbf{D}_{\mathbf{P}}^{-1/2} \mathbf{P} \mathbf{D}_{\mathbf{P}}^{-1/2} \right) \right\|_F.$$

The identity terms cancel, giving:

$$\|\mathcal{L}_{\mathbf{F}} - \mathcal{L}_{\mathbf{P}}\|_F = \left\| \mathbf{D}_{\mathbf{P}}^{-1/2} \mathbf{P} \mathbf{D}_{\mathbf{P}}^{-1/2} - \mathbf{D}_{\mathbf{F}}^{-1/2} \mathbf{F} \mathbf{D}_{\mathbf{F}}^{-1/2} \right\|_F.$$

We add and subtract $\mathbf{D}_{\mathbf{F}}^{-1/2} \mathbf{P} \mathbf{D}_{\mathbf{F}}^{-1/2}$ to decompose the expression:

$$\|\mathcal{L}_{\mathbf{F}} - \mathcal{L}_{\mathbf{P}}\|_F \leq \left\| \mathbf{D}_{\mathbf{F}}^{-1/2} \mathbf{F} \mathbf{D}_{\mathbf{F}}^{-1/2} - \mathbf{D}_{\mathbf{F}}^{-1/2} \mathbf{P} \mathbf{D}_{\mathbf{F}}^{-1/2} \right\|_F + \left\| \mathbf{D}_{\mathbf{F}}^{-1/2} \mathbf{P} \mathbf{D}_{\mathbf{F}}^{-1/2} - \mathbf{D}_{\mathbf{P}}^{-1/2} \mathbf{P} \mathbf{D}_{\mathbf{P}}^{-1/2} \right\|_F.$$

Denote the two terms above as (A) and (B), respectively.

Term (A): Difference due to affinity matrices.

Since $\mathbf{D}_{\mathbf{F}}^{-1/2}$ is fixed in this term, we can factor it out:

$$(A) = \left\| \mathbf{D}_{\mathbf{F}}^{-1/2} (\mathbf{F} - \mathbf{P}) \mathbf{D}_{\mathbf{F}}^{-1/2} \right\|_F \leq \|\mathbf{D}_{\mathbf{F}}^{-1/2}\|^2 \cdot \|\mathbf{F} - \mathbf{P}\|_F.$$

Let $\lambda_{\min}(\mathbf{D}_{\mathbf{F}})$ denote the minimum diagonal entry of $\mathbf{D}_{\mathbf{F}}$. Then $\|\mathbf{D}_{\mathbf{F}}^{-1/2}\| = \lambda_{\min}(\mathbf{D}_{\mathbf{F}})^{-1/2}$, and assuming $\lambda_{\min}(\mathbf{D}_{\mathbf{F}}) \geq d_{\min} > 0$, we obtain:

$$(A) \leq \frac{1}{d_{\min}} \cdot \epsilon.$$

Term (B): Difference due to degree normalization.

We now bound the difference caused by changing from $\mathbf{D}_{\mathbf{F}}$ to $\mathbf{D}_{\mathbf{P}}$ in the normalization. Define $g(\mathbf{D}) := \mathbf{D}^{-1/2} \mathbf{P} \mathbf{D}^{-1/2}$. Using matrix perturbation theory (see *e.g.*, Kato's inequality or Fréchet derivatives of matrix functions):

$$\mathbf{D}_{\mathbf{P}}^{-1/2} \mathbf{P} \mathbf{D}_{\mathbf{P}}^{-1/2} \approx \mathbf{D}_{\mathbf{F}}^{-1/2} \mathbf{P} \mathbf{D}_{\mathbf{F}}^{-1/2} + \nabla g(\mathbf{D}_{\mathbf{F}}) [\mathbf{D}_{\mathbf{P}} - \mathbf{D}_{\mathbf{F}}],$$

and assuming the matrices are close and well-conditioned, we can approximate:

$$(B) \approx \|\nabla g(\mathbf{D}_{\mathbf{F}}) [\mathbf{D}_{\mathbf{P}} - \mathbf{D}_{\mathbf{F}}]\|_F \leq C' \cdot \|\mathbf{D}_{\mathbf{P}} - \mathbf{D}_{\mathbf{F}}\| = C' \delta,$$

where C' depends on the norm of \mathbf{P} and the conditioning of $\mathbf{D}_{\mathbf{F}}$.

Combining (A) and (B), we obtain:

$$\|\mathcal{L}_{\mathbf{F}} - \mathcal{L}_{\mathbf{P}}\|_F \leq \frac{1}{d_{\min}} \cdot \epsilon + C' \cdot \delta,$$

which can be rewritten as:

$$\|\mathcal{L}_{\mathbf{F}} - \mathcal{L}_{\mathbf{P}}\|_F \leq C(\epsilon + \delta),$$

where C is a constant depending on d_{\min}^{-1} , $\|\mathbf{P}\|$, and graph sparsity. \square

Corollary 2. *The GCR alignment loss, which encourages $\|\mathbf{F} - \mathbf{P}\|_F \leq \epsilon$, indirectly enforces spectral similarity of the normalized Laplacians. This promotes agreement between the clustering structure and diffusion properties of the learned features and masked predictions.*

E.3 PAC-Bayesian View of Structural Regularization

We now present a PAC-Bayesian interpretation of GCR. The PAC-Bayes framework provides a probabilistic approach to generalization by relating the expected loss of a stochastic predictor to its empirical loss and the divergence between a posterior and a prior distribution over the hypothesis class.

Let \mathcal{P} denote a prior distribution over model functions f , representing a structure-agnostic belief (e.g., uniform or isotropic Gaussian over parameters). Let \mathcal{Q} be a posterior distribution supported on models that minimize training loss while also conforming to a structural constraint induced by GCR, i.e., \mathcal{Q} is restricted to functions f such that $\mathcal{L}_{\text{GCR}}^{(l)} \leq \epsilon$ for each relevant layer l .

Theorem 5 (PAC-Bayes Generalization Bound with GCR). *Let $\mathcal{L}(f) = \mathbb{E}_{(x,y) \sim \mathcal{D}}[\ell(f(x), y)]$ be the expected population loss of model f and let $\hat{\mathcal{L}}(f) = \frac{1}{n} \sum_{i=1}^n \ell(f(x_i), y_i)$ be the empirical loss on n training examples. Then, for any posterior distribution \mathcal{Q} over functions and any prior distribution \mathcal{P} , with probability at least $1 - \delta$ over the training data, the following bound holds:*

$$\mathbb{E}_{f \sim \mathcal{Q}}[\mathcal{L}(f)] \leq \mathbb{E}_{f \sim \mathcal{Q}}[\hat{\mathcal{L}}(f)] + \sqrt{\frac{\text{KL}(\mathcal{Q} \parallel \mathcal{P}) + \log(1/\delta)}{2n}}. \quad (21)$$

This classical PAC-Bayesian bound quantifies generalization via two key components:

- i. The empirical performance of models sampled from the posterior \mathcal{Q} .
- ii. The Kullback-Leibler (KL) divergence $\text{KL}(\mathcal{Q} \parallel \mathcal{P})$ between the posterior and the prior, which acts as a measure of how far \mathcal{Q} deviates from the prior belief.

In the context of GCR, we interpret the constraint $\mathcal{L}_{\text{GCR}}^{(l)} \leq \epsilon$ as imposing structure on the feature space. Specifically, GCR encourages the pairwise feature similarity matrix $\mathbf{F}^{(l)}$ at each layer to align with the semantic structure encoded in \mathbf{P} (e.g., class-level affinity). This alignment can be viewed as an inductive bias or structural preference.

Assuming \mathcal{Q} is supported only on models satisfying $\mathcal{L}_{\text{GCR}}^{(l)} \leq \epsilon$, we argue that the complexity term $\text{KL}(\mathcal{Q} \parallel \mathcal{P})$ is influenced by the degree of this alignment.

Proposition 7 (Structure-Induced KL Complexity). *If the posterior \mathcal{Q} is concentrated on models with small GCR loss at layer l , then the KL divergence to an isotropic prior \mathcal{P} satisfies:*

$$\text{KL}(\mathcal{Q} \parallel \mathcal{P}) \leq C \sum_l \|\mathbf{F}^{(l)} - \mathbf{P}\|_F^2, \quad (22)$$

for some constant C depending on the form of \mathcal{P} .

Sketch of argument. Let us assume that \mathcal{P} is a structure-agnostic prior, e.g., an isotropic Gaussian over parameters or functions. Now suppose \mathcal{Q} is supported on models where the GCR loss is small. Since $\mathcal{L}_{\text{GCR}}^{(l)}$ penalizes deviation between the normalized feature similarity matrix $\mathbf{F}^{(l)}$ and the semantic affinity matrix \mathbf{P} , this implies that models in the support of \mathcal{Q} induce feature geometries that respect the semantic structure.

From an information-theoretic perspective, concentrating the posterior on such structured models induces a regularization effect: it reduces the space of allowable hypotheses compared to the unconstrained prior. Intuitively, this compression is captured by the KL divergence. Since the GCR loss explicitly penalizes misalignment, its cumulative value over layers effectively bounds the information-theoretic complexity:

$$\text{KL}(\mathcal{Q} \parallel \mathcal{P}) \lesssim \sum_l \|\mathbf{F}^{(l)} - \mathbf{P}\|_F^2.$$

More formally, this can be justified using PAC-Bayesian compression bounds or Gaussian complexity arguments, which show that the KL divergence scales with the squared norm of the constraint function, in this case, the Frobenius norm between affinity matrices. \square

Remark 5. *This perspective reveals that GCR does more than minimize training loss, it also implicitly regularizes the hypothesis space by favoring models whose internal representations reflect known semantic structure. This improves generalization by reducing the effective size of the model class, as made explicit through the PAC-Bayesian framework.*

F Analysis of GCR’s Time Complexity

Below, we present a theoretical analysis of the GCR’s time complexity per training iteration, from both a naïve computational perspective and an optimized parallel execution view.

Feature graph construction. At each layer $l = 1, \dots, K$ where a GCL is applied, a feature similarity graph $\mathbf{F}^{(l)} \in \mathbb{R}^{n \times n}$ is constructed using the cosine similarity. We have time complexity: (i) Naïve (sequential compute): Normalizing all n feature vectors costs $\mathcal{O}(nd)$; pairwise cosine similarities require $\mathcal{O}(n^2d)$. (ii) GPU-parallelized: With sufficient vector-level parallelism, normalization and similarity computations can be reduced to $\mathcal{O}(\log d)$, assuming parallel dot products. (iii) Total over K layers: $\mathcal{O}(K \cdot \log d_{\max})$, where d_{\max} is the largest feature dimension across all GCL layers.

Prediction graph construction. The prediction graph $\mathbf{P} \in \mathbb{R}^{n \times n}$ is derived from softmax-normalized logits $\mathbf{z}_i \in \mathbb{R}^C$. We have time complexity: (i) Naïve (sequential compute): Softmax computation costs $\mathcal{O}(nC)$, cosine similarities $\mathcal{O}(n^2C)$, and masking $\mathcal{O}(n^2)$. (ii) GPU-parallelized: Per-sample operations reduce to $\mathcal{O}(\log C)$, and masking becomes $\mathcal{O}(1)$ due to element-wise matrix operations.

Graph alignment loss. The loss at each layer measures the Frobenius norm of the difference between graphs: $\mathcal{L}_{\text{GCR}}^{(l)} = \|\text{triu}(\mathbf{F}^{(l)} - \mathbf{P})\|_F^2$. We have time complexity: (i) Naïve (sequential compute): $\mathcal{O}(n^2)$, (ii) GPU-parallelized: $\mathcal{O}(\log n)$, assuming reduction over parallel threads for norm computation.

Adaptive weighting across layers. If adaptive weighting (Eq. 6) is used, normalized weights are computed for each layer based on alignment discrepancy. We have time complexity: $\mathcal{O}(Kn^2)$, where K is the number of GCL-applied layers.

Total time complexity. (i) Naïve (sequential compute): Assuming GCLs are applied at K layers, with d_{\max} being the maximum feature dimension and C the number of classes: $\mathcal{O}(K \cdot n^2(d_{\max} + C))$, with the dominant term $\mathcal{O}(n^2d_{\max})$ due to high-dimensional pairwise feature similarity computations. (ii) GPU-Parallelized: With parallel compute, complexity reduces to $\mathcal{O}(K \cdot (\log d_{\max} + \log C))$, where $\log C \ll \log d_{\max}$ can be ignored. If n^2 is too large to fit into memory, the computation can be split into s sequential parallel blocks (e.g., $s = 4$).

Practical considerations and optimizations. (i) Scalability: GCR operates on batches rather than entire datasets. Its quadratic cost in n (e.g., $n = 128$) is modest in practice. (ii) Parallel efficiency: All computations are matrix-based and benefit from hardware acceleration. Libraries such as PyTorch exploit thread and GPU-level parallelism to accelerate operations like `torch.bmm`, `functional.cosine_similarity`, and `torch.triu`. (iii) Zero parameter overhead: GCR introduces no trainable parameters and does not affect memory footprint or gradient flow.

GCR introduces a lightweight yet effective form of structure-based regularization, with per-layer complexity no more than $\mathcal{O}(\log d)$. Thanks to batch-local operation, GPU-friendly computations, and absence of learnable parameters, GCR scales efficiently while improving semantic alignment.

G Experimental Setup

We evaluate the effectiveness and efficiency of GCR across a diverse range of image classification benchmarks and model architectures. All experiments are conducted on NVIDIA V100 GPUs (32GB) paired with 12 CPU cores and 48GB of system RAM.

For convolutional architectures trained on CIFAR-10 and CIFAR-100, we follow the standard training protocol from [25]. Specifically, models are trained for 200 epochs using stochastic gradient descent with Nesterov momentum of 0.9 and weight decay of 5×10^{-4} . The initial learning rate is set to 0.1 and decayed by a factor of 5 at epochs 60, 120, and 160. We use a fixed batch size of 128 for all training. The GCR loss is incorporated with a regularization weight of $\lambda = 1$ unless otherwise stated.

For Masked Autoencoder (MAE) experiments on CIFAR-10 and CIFAR-100, we also use the same hardware setup. The ViT-Tiny encoder is pre-trained for 2200 epochs with a 75% masking ratio. Optimization uses AdamW with a base learning rate of 1.5×10^{-4} (scaled by global batch size), weight decay of 0.05, a 200-epoch linear warm-up, and cosine decay. A global batch size of 4096 is realized via gradient accumulation with a device batch size of 512, repeated eight times before each

optimizer step. Training uses automatic mixed precision (AMP) and gradient norm clipping at 1.0, completing pre-training in approximately 13 hours and 40 minutes.

The pretrained ViT-Tiny encoder is then fine-tuned for classification over 200 epochs using AdamW with a base learning rate of 1×10^{-3} (scaled by batch size), weight decay 0.05, a 10-epoch warm-up, and cosine decay. Fine-tuning uses a batch size of 128 without gradient accumulation or AMP. Fine-tuning times are 4 hours for the baseline and approximately 4 hours 40 minutes with GCR.

We evaluate GCR on eight convolutional neural networks on CIFAR-100, including MobileNet, SqueezeNet, ShuffleNet, ResNet-34, ResNet-50, ResNeXt-50, ResNeXt-101, and DenseNet-121. For CIFAR-10, we include GoogLeNet and ResNet-101, totaling ten models. Incorporating GCR results in a modest increase in training time due to graph construction and alignment overhead. For example, MobileNet and SqueezeNet baseline trainings take approximately 45 minutes each, increasing to 60 and 80 minutes with GCR, respectively. ShuffleNet increases from 140 to 170 minutes, ResNet-34 from 160 to 280 minutes, ResNet-50 and ResNeXt-50 from around 210 to 390 and 230 to 400 minutes, respectively. Larger models such as ResNeXt-101 and DenseNet-121 see increases from 420 to 540 minutes and 270 to 330 minutes. GoogLeNet runs 125 minutes baseline and 140 minutes with GCR; ResNet-101 increases from 300 to 370 minutes.

On Tiny ImageNet, we test GCR on four transformer models (ViT, Swin Transformer, MobileViT, CEiT) and four CNNs (MobileNet, ResNet, SE-ResNet, Stochastic ResNet). CNNs are trained for 200 epochs with initial learning rate 0.1 (decayed at epochs 60/120/160), batch size 128, weight decay 5×10^{-4} , and momentum 0.9. Transformers use AdamW optimizer with initial learning rate 1×10^{-4} , weight decay 5×10^{-2} , and cosine annealing decay to 1×10^{-6} , including a 10-epoch warm-up. Transformers are trained for 250 epochs with batch size 256, using AMP for efficiency and gradient clipping with max norm 1.0.

Training times increase moderately when applying GCR. MobileNet’s training grows from 3 to 4 hours, ResNet-34 from 16 to 19.5 hours, SE-ResNet-18 from 10 hours 40 minutes to 12 hours, and StochasticDepth-18 from 8 to 9.5 hours. For transformers, ViT-B/16 requires 15 hours baseline and 20 hours with GCR, ViT-B/32 from 6 to 7.5 hours, MobileViT-S from 9 hours 15 minutes to 10.5 hours, MobileViT-XS from 8 to 9 hours, MobileViT-XXS from 5 hours 40 minutes to 6.5 hours, Swin Transformer-Tiny from 13 to 16 hours, and CEiT-Tiny from 8 hours 10 minutes to 10 hours.

Overall, GCR introduces a consistent yet manageable computational overhead across architectures, primarily due to graph construction and alignment. All reported training times are averages over three independent runs with varying random seeds to ensure reproducibility. GCR adds no trainable parameters and is designed for parallel execution on modern hardware, maintaining efficient and scalable training.

H Additional Results and Visualizations

H.1 t-SNE Visualizations

We present a comparison of t-SNE visualizations for baseline models and their GCL-augmented counterparts on CIFAR-10 in Fig. 7.

In models enhanced with GCL (Figs. 7b, 7d and 7f, semantically related classes, such as Airplane, Ship, and Truck (all vehicles), form tighter groupings, indicating that GCL promotes a better understanding of high-level semantic concepts. A similar effect is observed among animal classes like Dog, Cat, Horse, and Deer.

These improvements are consistent across diverse architectures, including MobileNet, ResNet-34, and MAE, highlighting the generality and robustness of GCL. Rather than overfitting to a specific architecture, GCL contributes to relational feature learning in a model-agnostic and parameter-free manner.

H.2 Effect of Batch Size in GCR Framework

Batch size plays a critical role in the effectiveness of GCR, as both the feature and prediction relational graphs are constructed at the batch level. To study this impact, we conduct experiments using the Masked Autoencoder (MAE) model and visualize the prediction graphs across varying

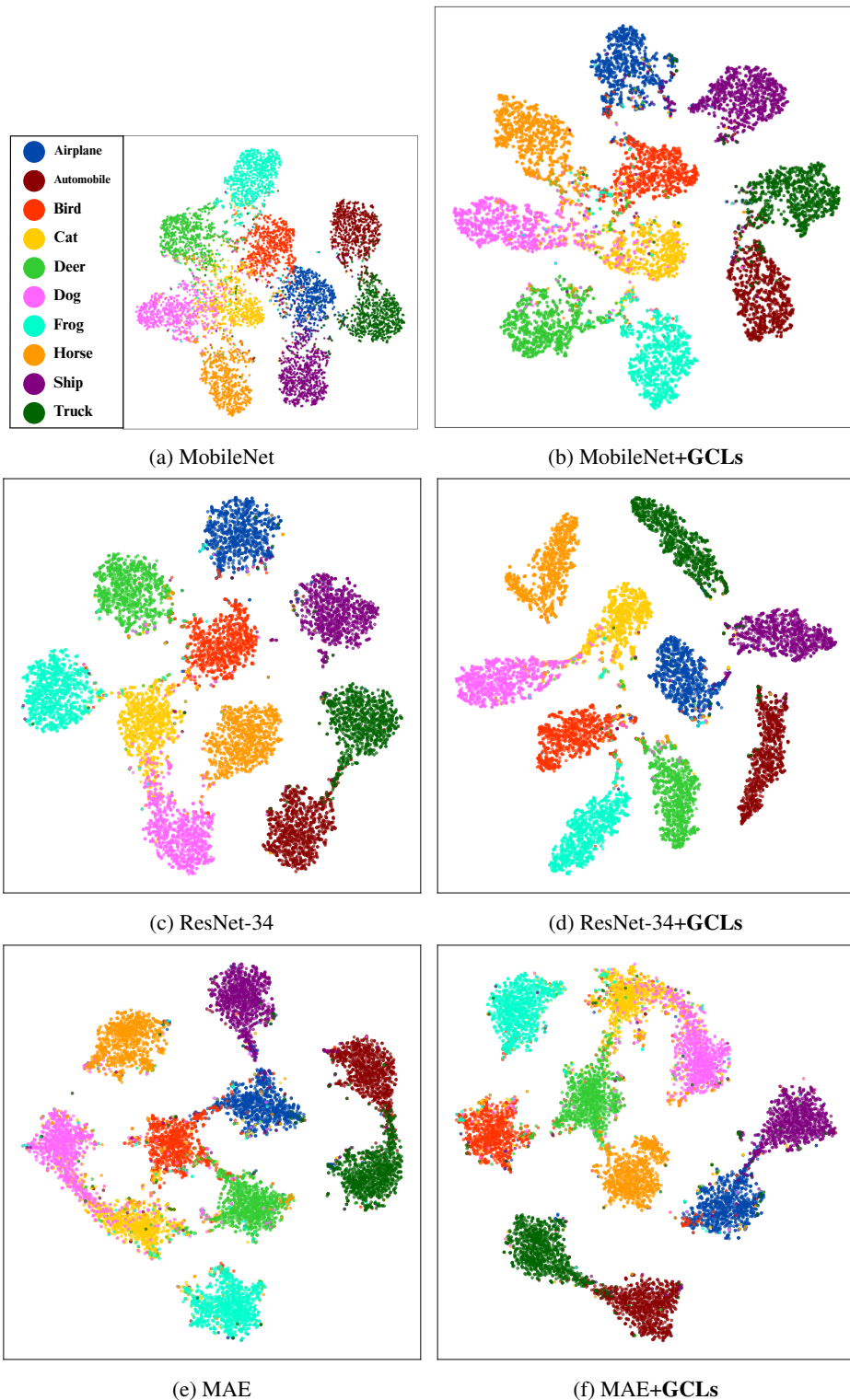


Figure 7: t-SNE visualizations of feature representations on CIFAR-10. (Left) Original model architectures; (Right) corresponding GCL-augmented models. Our method consistently enhances feature structure across diverse architectures, including MobileNet, ResNet-34, and MAE (with ViT-Tiny encoder), by yielding tighter intra-class clusters and improved inter-class separation. Notably, **GCR distinctly separates semantic groups such as animals and vehicles** (*e.g.*, (e) vs. (f)). Importantly, GCL is lightweight and introduces no additional parameters.

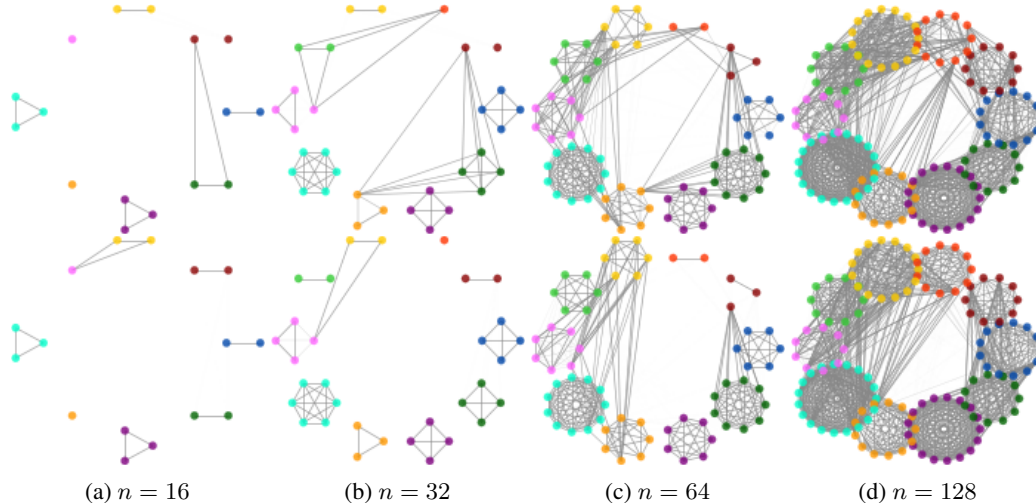


Figure 8: Effect of batch size (n) in the GCR framework. We evaluate using the Masked Autoencoder model. The top row shows the baseline; the bottom row shows the GCL-augmented counterpart. From left to right, the relational graphs are constructed on softmax predictions as n increases from 16 to 128. As batch size grows, GCL-augmented models consistently exhibit tighter intra-class clusters and clearer inter-class separation.

batch sizes ($n \in \{16, 32, 64, 128, 256, 512\}$). We compare the baseline and GCL-augmented versions side-by-side, focusing on the structure of the similarity graphs derived from softmax outputs.

Qualitative evaluation. Fig. 8 illustrates these results. In the top row (baseline), increasing batch size introduces more noise and inter-class confusion, especially at smaller n , where limited sample diversity can distort the global structure. As batch size increases, the prediction graphs become more complete but remain noisy and less structured, indicating that larger batches alone do not guarantee better semantic organization.

In contrast, the bottom row (GCL-augmented) shows that our method consistently yields more coherent relational graphs across all batch sizes. Even at smaller n , GCR promotes more compact intra-class clusters and better inter-class separation. At larger n , the effect is even more pronounced, as the graph-based alignment uses the increased pairwise statistics to further regularize feature space according to prediction semantics.

As shown in Fig. 8, GCR remains effective across a wide range of batch sizes. Even with small batches (*e.g.*, $n = 16$ and $n = 32$), GCL-enhanced models produce more coherent intra-class clusters and stronger inter-class separation than the baseline. This supports our claim that GCR can extract meaningful structure even from limited relational signals.

These observations highlight two important insights: (i) GCR is robust to batch size and can extract meaningful structure even from smaller batches, and (ii) larger batches enhance the graph alignment process by providing richer relational signals, amplifying the benefits of GCR. This makes our method especially suitable for modern hardware and large-scale distributed training setups where large batches are common.

Quantitative evaluation. While larger batches amplify gains by providing denser graphs, they are not essential. Table 5 confirms consistent performance improvements across batch sizes on both CIFAR-10 (ShuffleNet) and Tiny ImageNet (CeiT). These results affirm GCR’s robustness and flexibility, even in resource-constrained or small-batch training setups.

H.3 Measuring Similarity

We chose cosine similarity to emphasize directional alignment, which is more semantically meaningful and robust to nuisance factors (*e.g.*, brightness) than raw magnitude. This aligns with common practice in representation learning, where angular relationships often capture class structure more effectively.

Table 5: Effect of batch size on GCR performance for ShuffleNet (CIFAR-10) and CeiT (Tiny ImageNet).

ShuffleNet on CIFAR-10			CeiT on Tiny ImageNet		
Batch Size	+ GCR	Baseline	Batch Size	+ GCR	Baseline
16	79.90±0.38	78.88±0.41	16	44.84±0.31	43.78±0.35
32	87.91±0.36	86.91±0.37	32	47.55±0.29	46.89±0.31
64	91.26±0.25	90.64±0.35	64	49.19±0.25	48.09±0.30
128	92.79±0.20	91.21±0.28	128	51.22±0.20	49.95±0.29
256	92.89±0.25	92.07±0.27	256	50.77±0.19	49.62±0.24
512	92.33±0.23	91.94±0.25	512	50.65±0.22	49.34±0.24

Table 6: Performance comparison of different GCL integration strategies with various kernels.

Method	Cosine	RBF	Polynomial	Sigmoid	Laplacian
Baseline	65.95±0.25	65.95±0.25	65.95±0.25	65.95±0.25	65.95±0.25
Early GCL	67.53±0.21	66.66±0.28	66.59±0.29	66.63±0.30	66.42±0.28
Mid GCL	67.91±0.19	67.04±0.24	66.97±0.24	67.01±0.36	66.80±0.29
Late GCL	68.32±0.20	67.45±0.23	67.38±0.29	67.42±0.29	67.21±0.31
Early + Mid	67.62±0.23	66.75±0.24	66.68±0.21	66.72±0.27	66.51±0.29
Mid + Late	68.26±0.18	67.39±0.23	67.32±0.23	67.36±0.31	67.15±0.27
Early + Late	67.21±0.24	66.34±0.21	66.27±0.28	66.31±0.28	66.10±0.26
Full GCL	68.25±0.21	67.38±0.22	67.31±0.25	67.35±0.27	67.14±0.25

While kernel methods (*e.g.*, RBF, polynomial) offer expressive similarity functions, our GCLs operate on features already shaped by deep non-linear transformations. Thus, we prioritize simplicity and generality: cosine is efficient, *hyperparameter-free*, and preserves our goal of making GCLs a lightweight, plug-and-play regularizer.

We tested multiple kernels on MobileNet with CIFAR-100 and found cosine consistently outperforms others, further supporting our design choice.

H.4 GCR Reduces Inter-Class Noise

We now provide quantitative evidence supporting our claim that GCR reduces inter-class noise, beyond prior visualizations.

Clustering and separability metrics. We use the Silhouette score (higher values indicate tighter intra-class clustering and clearer separation from other classes) and the Separability ratio (measuring inter-class *vs.* intra-class distance; higher is better).

Results on CIFAR-10 across ten models show that GCR consistently improves feature separability and cohesion. For example, on ResNet-34, Silhouette(\uparrow) increases from 0.60 to 0.73, and SepRatio(\uparrow) from 3.10 to 4.41, confirming clearer class boundaries.

Confusion matrices. Confusion matrices indicate reduced inter-class confusion. For example, “cat-dog” confusion decreases from 0.09 to 0.07, and diagonal accuracies improve across several classes (*e.g.*, “auto”: 0.96 \rightarrow 0.97).

H.5 GCR on Earlier Layers

Motivation for early-layer regularization. While later layers are more semantic, we find that GCR sometimes works best in earlier layers, especially on Tiny ImageNet and low-capacity models. This effect arises due to several factors. Early features often exhibit higher noise and misalignment, which GCR’s adaptive weighting naturally targets. Regularization at these layers helps prune spurious low-level features, setting the network on a better optimization path. Moreover, prediction-driven self-prompting allows final-layer structure to refine earlier layers via backpropagated relational

Table 7: Quantitative metrics showing improvements in feature clustering and confidence with GCR.

Model	Silhouette		SepRatio		Confidence	
	Baseline	+ GCR	Baseline	+ GCR	Baseline	+ GCR
DenseNet-121	0.4724	0.5001	2.2278	2.3325	0.9746	0.9805
ShuffleNet	0.2806	0.4083	1.7692	2.0472	0.9568	0.9619
SqueezeNet	-0.1245	-0.0825	1.0008	1.0494	0.9603	0.9660
ResNet-34	0.6032	0.7314	3.1015	4.4144	0.9801	0.9870
ResNet-50	0.5314	0.6186	2.5480	3.2294	0.9789	0.9835
ResNet-101	0.5641	0.6069	2.7705	3.0793	0.9803	0.9859
ResNeXt-50	0.5298	0.5604	2.6323	2.7941	0.9788	0.9814
ResNeXt-101	0.5668	0.6951	2.8387	3.8703	0.9811	0.9880
GoogLeNet	-0.0255	-0.0055	1.1982	1.2065	0.9720	0.9749
Avg	0.3776	0.4481	2.2319	2.6692	0.9737	0.9788

Table 8: CIFAR-10 confusion matrix for the baseline model.

	plane	auto	bird	cat	deer	dog	frog	horse	ship	truck
plane	0.93	0.01	0.02	0.01					0.03	0.01
auto	0.01	0.96								0.03
bird	0.02		0.88	0.03	0.02	0.01	0.02	0.01		
cat	0.01		0.02	0.83	0.02	0.08			0.01	0.01
deer	0.01		0.01	0.02	0.93	0.01	0.01	0.01		
dog			0.01	0.09	0.02	0.86		0.01		
frog	0.01		0.02	0.01	0.01		0.95			
horse			0.01	0.02	0.01	0.02		0.94		
ship	0.02	0.01							0.95	0.01
truck	0.01	0.04						0.01		0.94

Table 9: CIFAR-10 confusion matrix for the model **with GCR**.

	plane	auto	bird	cat	deer	dog	frog	horse	ship	truck
plane	0.94		0.02	0.01					0.01	0.01
auto		0.97								0.02
bird	0.01		0.89	0.03	0.02	0.02	0.01	0.01		
cat	0.01		0.01	0.85	0.01	0.08		0.01	0.01	0.01
deer	0.01		0.01	0.02	0.94	0.01	0.01	0.01		
dog			0.01	0.07	0.01	0.88		0.01		
frog	0.01		0.02	0.01	0.01		0.95			
horse			0.01	0.02	0.01	0.01		0.94		
ship	0.02								0.96	0.01
truck	0.01	0.02		0.01					0.01	0.95

Table 10: Impact of early *vs.* late GCR on feature robustness in ShuffleNet. Pre-freeze and post-freeze top-1 accuracy are reported, along with the performance drop.

Model	Pre-freeze	Post-freeze	Performance Drop
Model A (Early-GCR)	66.8%	66.1%	0.7%
Model B (Late-GCR)	66.4%	65.1%	1.2%

Table 11: Performance comparison on CIFAR-10, CIFAR-100, and ImageNet-1K.

Method	CIFAR-10	CIFAR-100	ImageNet-1K
ResNet-18			
CNN2GNN [101]	95.51±0.42	74.80±0.81	60.12±1.02
CNN2GNN + GCR	95.87±0.31	76.23±0.38	62.47±0.47
CNN2Transformer [101]	95.79±0.24	77.39±0.20	71.12±0.35
CNN2Transformer + GCR	95.96±0.35	78.23±0.30	72.33±0.31
ResNet-34			
CNN2GNN [101]	96.39±0.41	77.87±0.91	61.02±0.77
CNN2GNN + GCR	96.67±0.36	78.14±0.54	62.88±0.46
CNN2Transformer [101]	96.73±0.37	80.10±0.45	75.42±0.15
CNN2Transformer + GCR	96.97±0.36	81.27±0.29	76.67±0.26

signals. Shallow models benefit more from early guidance because they downsample aggressively and lack strong inductive biases.

Experiments and analysis. To test whether GCR’s impact correlates with a layer’s semantic misalignment, we trained a CeiT model on Tiny ImageNet without GCR and measured the baseline discrepancy for each block l : $\delta(l) = \|\mathbf{F}^{(l)} - \mathbf{P}\|_F^2$. We then applied GCR to individual blocks and recorded the top-1 accuracy gain $\Delta\text{Acc}(l)$. Results show that early layers, bridging low-level features to class concepts, exhibit the highest misalignment and largest gains: (i) Block 1: $\delta_1 = 0.45$, gain +1.2%, (ii) Block 2: $\delta_2 = 0.30$, gain +0.9%. A strong Pearson correlation of 0.62 between $\{\delta(l)\}$ and $\{\Delta\text{Acc}(l)\}$ quantitatively confirms that GCR is more effective where feature-prediction misalignment is greater.

Next, we evaluated whether early GCR creates more robust features that benefit later layers, producing a “feature cleaning” effect. We trained two ShuffleNet models (5 blocks each) and then froze the regularized blocks to assess their standalone quality: (i) Model A (Early-GCR): GCLs on Blocks 1-2, frozen after 100 epochs, then fine-tuned remaining blocks. (ii) Model B (Late-GCR): GCLs on Blocks 4-5, frozen and fine-tuned similarly. Model A’s smaller drop indicates that early GCR features are more robust and semantically coherent, reducing dependence on later-stage regularization (Table 10). In contrast, Model B’s larger drop suggests that late-GCR performance relies heavily on continued regularization, with earlier features remaining entangled.

These results show that GCR scales well and confirm our core insight: aligning feature geometry with prediction semantics strengthens generalization.

H.6 Results on CIFAR-10, CIFAR-100, and ImageNet-1K

Distinction from graph-based methods. Although graph-based methods have been extensively studied, our proposed GCR departs from this line of work by introducing a fundamentally different mechanism. Existing approaches often depend on static external graphs or rely on iterative message passing as in GNNs. By contrast, GCR uses a novel self-prompted regularization strategy, where the model’s own predictions dynamically construct a class-aware graph that supervises its intermediate feature representations.

This design brings several innovations. First, instead of relying on pre-defined structures or memory banks, GCR builds graphs on the fly from the model’s softmax outputs within each batch, making the supervision inherently adaptive to the evolving state of the model. Second, GCR operates as a purely parameter-free regularizer rather than as a feature transformer. It introduces no additional learnable parameters, remains agnostic to architecture, and can be seamlessly integrated into diverse models with minimal overhead. Finally, GCR enforces a unique cross-space alignment: similarity graphs in the feature space are aligned with semantic graphs in the prediction space, coupling representation learning with prediction dynamics. In this way, GCR turns predictions into structured supervisory signals that guide feature learning, offering a lightweight yet powerful alternative to conventional graph-based classification methods.

Table 12: Results on ImageNet-1K.

Model	ViG-Ti [37]	ViG-Ti + GCR	ViG-S [37]	ViG-S + GCR	ViG-B [37]	ViG-B + GCR
Accuracy	73.9	74.9	80.4	81.7	82.3	84.0

Table 13: Comparison of GCR with one-hot labels vs. soft predictions on CIFAR-100 (average over 10 runs).

	MobileNet	ShuffleNet	SqueezeNet
Baseline	65.95±0.25	70.11±0.30	69.43±0.27
GCR (one-hot labels)	67.35±0.24	71.28±0.26	70.49±0.25
GCR (soft predictions, ours)	68.32±0.20	71.96±0.27	71.03±0.24

We provide direct comparisons between our GCR-augmented models and recent graph-based classification methods across CIFAR-10, CIFAR-100, and ImageNet-1K (Table 11 and Table 12).

The results clearly show the consistent and complementary benefits of GCR when integrated into graph-based backbones. They highlight key insights: (i) Consistent across architectures: GCR improves performance across diverse backbones (CNN2GNN [101], CNN2Transformer [101], ViG [37]), demonstrating broad applicability. (ii) Complementary to existing methods: Its self-regularization mechanism enhances CNN2GNN and CNN2Transformer, indicating orthogonality to existing graph-based pipelines. (iii) Scalable to large-scale tasks: Notable gains on ImageNet-1K (*e.g.*, +1.7% with ViG-B) show GCR’s effectiveness in complex, real-world settings. (iv) Lightweight and model-agnostic: GCR introduces no extra parameters and integrates easily into existing architectures.

Together, these findings reinforce GCR’s novelty and practical value as a flexible, self-prompted regularization framework applicable across scales and architectures.

H.7 Feature Similarity and the Information Bottleneck

Soft predictions vs. one-hot labels. For a pair of features \mathbf{f}_i and \mathbf{f}_j (dropping ReLU for brevity), we encourage $\cos(\mathbf{f}_i, \mathbf{f}_j) \approx \cos(\mathbf{s}_i, \mathbf{s}_j)$, where \mathbf{s}_i and \mathbf{s}_j are soft scores, not one-hot labels. These soft scores allow intra-class variations to persist while emphasizing task-relevant semantics. By imposing this constraint, we create an information bottleneck: the smaller the angle between \mathbf{f}_i and \mathbf{f}_j , the stronger the bottleneck. The network is thus forced to encode the most important variations while discarding nuisance factors. For example, in the Chihuahua vs. Great Dane scenario, features such as eyes, paws, nose, nails, and teeth are emphasized and encoded consistently across all dog species, whereas leg size or body shape variations are considered less relevant. This ensures that salient features are accurately captured and distinguishable across classes. If \mathbf{x}_i and \mathbf{x}_j belong to different classes (*e.g.*, dog vs. wolf), $\cos(\mathbf{s}_i, \mathbf{s}_j)$ will be lower but typically greater than zero, allowing some semantic similarity while relaxing the information bottleneck.

Using $\cos(\mathbf{f}_i, \mathbf{f}_j) \approx \cos(\mathbf{y}_i, \mathbf{y}_j)$ with one-hot labels would collapse intra-class variations (see Table 13). Instead, using soft predictions $\cos(\mathbf{f}_i, \mathbf{f}_j) \approx \cos(\mathbf{s}_i, \mathbf{s}_j)$ allows sufficient variation to be encoded.

Prediction similarity and diverse substructures. Even in classes with diverse substructures, prediction similarity mandates feature similarity: (i) In CNNs, as one moves toward the classifier, layers become increasingly shift- and permutation-invariant. Thus, deeper layers filter nuisance factors irrelevant to the classification task. (ii) The information bottleneck ensures the network focuses on salient, task-relevant features and discards uninformative variations. (iii) The bottleneck strength is controlled by λ in Eq. (7). Moderate values ($\lambda = 1$) perform best (see Table 14).

Table 14: Impact of bottleneck strength λ on CIFAR-100 (ResNet-34).

λ	0	0.1	0.3	0.5	0.7	1	3	5	7	10
Top-1 Acc (%)	76.76	76.80	76.87	77.32	77.61	78.38	76.74	76.02	75.90	75.37

Table 15: Effect of varying τ on CIFAR-100 with ResNet-34.

τ	0	1e-5	1e-4	1e-3	1e-2
Accuracy	78.38	78.32	78.27	78.13	76.04

These results confirm that GCR preserves intra-class variations while enforcing focus on the most important semantic features, improving robustness and accuracy without collapsing representations.

H.8 Lipschitz Continuity and Our Mechanism

L -Lipschitz continuous networks. It is well established that enforcing L -Lipschitz continuity in a network, such as a discriminator, helps regularize its layers and prevents overfitting. For example, Lipschitz Generative Adversarial Nets (LGANs) [128], along with many subsequent works on classification and fine-tuning under L -Lipschitzness.

This condition can be imposed on feature vectors $\phi(\cdot)$ of a chosen layer l by design, leading to

$$\|\phi_l(\mathbf{x}) - \phi_l(\mathbf{x}')\|_2 \leq L\|\mathbf{x} - \mathbf{x}'\|_2, \quad \forall \mathbf{x}, \mathbf{x}' \in \mathcal{D}, \quad (23)$$

where L is the Lipschitz constant. Intuitively, if L is small, then a small input change $\mathbf{x} \rightarrow \mathbf{x}'$ produces a small change in the features $\phi_l(\mathbf{x}) \rightarrow \phi_l(\mathbf{x}')$, while a large change in input produces a proportionally large change in the features. This stabilizes the network response.

A practical way to encourage such behavior is through an auxiliary regularization loss added to the main task loss:

$$\mathbb{E}_{\mathbf{x}, \mathbf{x}'} (\|\phi_l(\mathbf{x}) - \phi_l(\mathbf{x}')\|_2 - L\|\mathbf{x} - \mathbf{x}'\|_2)^2, \quad (24)$$

which promotes the approximation

$$\|\phi_l(\mathbf{x}) - \phi_l(\mathbf{x}')\|_2 \approx L\|\mathbf{x} - \mathbf{x}'\|_2. \quad (25)$$

For simplicity, we omit ReLU and cosine similarity in what follows and use the ℓ_2 distance, though cosine distance can be incorporated without difficulty. We promote alignment of the form

$$\mathbb{E}_{\mathbf{x}, \mathbf{x}'} (\|\phi_l(\mathbf{x}) - \phi_l(\mathbf{x}')\|_2 - \beta\|s(\mathbf{x}) - s(\mathbf{x}')\|_2)^2, \quad (26)$$

where $s(\cdot)$ denotes the softmax score. This yields an information bottleneck of the form

$$\|\phi_l(\mathbf{x}) - \phi_l(\mathbf{x}')\|_2 \approx \beta\|s(\mathbf{x}) - s(\mathbf{x}')\|_2. \quad (27)$$

Combining the Lipschitz condition with our bottleneck mechanism, we obtain

$$L\|\mathbf{x} - \mathbf{x}'\|_2 \approx \|\phi_l(\mathbf{x}) - \phi_l(\mathbf{x}')\|_2 \approx \beta\|s(\mathbf{x}) - s(\mathbf{x}')\|_2, \quad (28)$$

which implies

$$\|s(\mathbf{x}) - s(\mathbf{x}')\|_2 \approx \frac{L}{\beta}\|\mathbf{x} - \mathbf{x}'\|_2. \quad (29)$$

This demonstrates that our model does not collapse intermediate features into identical representations. Instead, small input variations $\mathbf{x} \rightarrow \mathbf{x}'$ yield small variations in both features and softmax scores, while large input differences induce proportionally large differences in the outputs.

The strength of this relation depends on the network’s local L -Lipschitzness (which may be fixed or vary in non-Lipschitz networks) and the scaling factor β , which is implicitly controlled by our parameter λ . Therefore, our information bottleneck mechanism ensures stable yet discriminative feature variation.

Introducing τ : collapse prevention by design. We enforce $\angle(\phi_l(\mathbf{x}_i), \phi_l(\mathbf{x}_j)) > \tau$ by a simple soft penalty $\sum_l \mathbf{1}(y_i = y_j) \cdot \mathbf{1}(\angle(\phi_l(\mathbf{x}_i), \phi_l(\mathbf{x}_j)) < \tau) \cdot (\angle(\phi_l(\mathbf{x}_i), \phi_l(\mathbf{x}_j)) - \tau)^2$, where $\mathbf{1}(\cdot)$ is the indicator function (e.g., do samples i and j share the same label?) and $\angle(\mathbf{x}, \mathbf{y}) = \cos^{-1}\left(\frac{\mathbf{x}^\top \mathbf{y}}{\|\mathbf{x}\|_2 \cdot \|\mathbf{y}\|_2}\right)$.

The results for CIFAR-100 using ResNet-34 are in Table 15. This result directly offers both anti-collapse control and evidence that the best results are attained for $\tau = 0$ (not pushing angles of the same class apart). Always maintaining a non-zero angle, e.g., $\tau = 1e-2$, is worse. We therefore conclude that our network does not suffer from feature dimensional collapse. However, if such collapse did occur, it could be prevented by a simple penalty, as demonstrated here.

Table 16: Results on CIFAR-100 (100 classes) with MobileNet. Accuracy and intra-/inter-class variance across six layers under different τ .

τ (deg)	Acc	1st		2nd		3rd		4th		5th		6th	
		intra	inter	intra	inter	intra	inter	intra	inter	intra	inter	intra	inter
baseline	65.95	38.71	13.81	22.30	7.56	12.00	5.27	5.10	4.24	17.71	19.49	8.64	9.69
ours (0.00)	68.14	31.21	12.02	18.18	7.61	9.98	4.28	3.94	3.25	16.82	18.69	8.30	9.32
0.08	68.21	31.25	12.56	18.28	6.54	9.92	4.46	4.10	3.28	18.77	19.52	9.23	9.74
0.26	67.68	36.28	13.11	20.93	7.15	10.94	4.92	4.58	3.81	17.72	19.08	8.72	9.50
0.81	67.37	35.39	13.72	20.44	6.92	11.02	4.89	4.70	3.89	17.74	18.87	8.70	9.41
2.56	67.34	35.40	13.40	20.61	7.32	10.83	4.84	4.56	3.74	17.92	19.08	8.78	9.50
8.11	67.39	39.04	14.86	23.42	8.04	12.00	5.24	5.16	4.38	16.77	18.58	8.28	9.27

Table 17: Results on CIFAR-100 (20 super-classes) with MobileNet. Accuracy and intra-/inter-class variance across six layers under different τ .

τ (deg)	Acc	1st		2nd		3rd		4th		5th		6th	
		intra	inter	intra	inter	intra	inter	intra	inter	intra	inter	intra	inter
baseline	77.46	30.30	8.86	17.94	4.30	9.25	2.97	3.01	2.46	9.09	12.27	4.45	6.12
ours (0.00)	77.54	30.36	8.65	17.95	4.43	9.34	2.99	3.22	2.56	9.69	12.57	4.73	6.27
0.08	77.72	31.59	9.22	18.24	4.42	9.57	3.08	3.33	2.61	9.91	12.56	4.87	6.27
0.26	77.36	32.04	9.80	18.67	4.58	9.57	3.07	3.28	2.70	9.85	12.69	4.83	6.33
0.81	77.69	31.36	9.59	18.17	4.38	9.50	3.04	3.15	2.60	9.70	12.63	4.77	6.30
2.56	77.31	31.69	9.38	18.56	4.36	9.39	3.03	3.30	2.68	9.94	12.55	4.88	6.26
8.11	77.60	32.39	8.66	18.34	4.47	9.35	3.01	3.26	2.65	9.83	12.48	4.81	6.22

H.9 Preventing Dimensional Collapse by Design

Anti-collapse mechanism. We introduce a penalty to directly prevent by-design a possibility of dimensional collapse. To this end, we conduct an experiment on CIFAR-100, grouped into 20 super-classes, *e.g.*, vehicles (bicycle, bus, motorcycle, pickup truck, train), insects (bee, beetle, butterfly, caterpillar, cockroach), flowers (orchids, poppies, roses, sunflowers, tulips), *etc.*

To this end, we force the within-class angle \angle between pairs of features to be at least τ . Specifically, we add to our GCR loss the following soft penalty: $\beta \frac{1}{\zeta} \sum_l \mathbf{1}(y_i = y_j) \cdot \mathbf{1}(\angle(\phi_l(\mathbf{x}_i), \phi_l(\mathbf{x}_j)) < \tau) \cdot (\angle(\phi_l(\mathbf{x}_i), \phi_l(\mathbf{x}_j)) - \tau)^2$, which ensures that $\angle(\phi_l(\mathbf{x}_i), \phi_l(\mathbf{x}_j)) > \tau$ within each class. Here, ζ is a normalization factor accounting for counts of same-class elements. For cosine similarity, we also apply ReLU in the above equations to prevent negative angles.

Setup. We use pre-trained baselines for comparisons. For our model, we train GCR-augmented models on CIFAR-100 for: (i) the 100-class task, and (ii) the 20 super-class task. The GCR-augmented model is equipped with a by-design collapse prevention mechanism. We choose $\beta = 0.3$ (generally optimal in our experiments). Subsequently, we vary the minimum angle τ to enforce a lower bound on intra-class variance. We report both intra- and inter-class variance across all six layers of MobileNet (used for fast experiments), considering both the original 100 classes and the 20 super-classes. Additionally, we include a baseline comparison without applying our GCR framework.

Findings. The results on both the 100-class and 20-superclass tasks show that GCR improves accuracy while maintaining meaningful feature diversity. While enforcing a minimum within-class variance with $\tau = 0.08$ helps slightly, the variance for $\tau = 0.00$ (ours) never collapsed in our experiments and remains close to the best case $\tau = 0.08$. Importantly, setting larger τ values, which enforce large intra-class variance, degrades accuracy. Maintaining certain within-class feature variance by a soft penalty makes sense. At the same time, the dimensional collapse does not happen in our model even without that penalty.

I Limitations and Future Works

I.1 Failure Modes and Marginal Gains

Highly noisy data. GCR aligns feature graphs with a masked prediction graph, using it as a semantic reference. The quality of this reference is critical. Our method assumes reliable ground-truth labels

for the mask \mathbf{M} . If the training data contains spurious correlations or mislabeled examples, the alignment may reinforce these errors. Under high label noise, the prediction graph \mathbf{P} is based on a flawed mask, producing a corrupted supervisory signal that misguides feature representations toward incorrect semantics. This failure mode can lead to marginal gains or even performance degradation in our supervised framework.

Highly class-imbalanced data. Since GCR builds relational graphs at the batch level, the global context is limited to within-batch relationships. In highly imbalanced datasets, batches may contain few or no minority-class samples, resulting in sparse or uninformative prediction graphs for those classes. Consequently, the alignment loss is dominated by majority classes, potentially harming minority-class representations and leading to marginal overall gains.

Other scenarios leading to marginal gains. Beyond noisy and imbalanced data, GCR may yield marginal improvements in the following cases: (i) Simple datasets with high baseline performance: GCR targets noisy inter-class similarities and semantic structure. On simpler datasets with strong baseline models and well-separated features, there is less room for improvement. Our results confirm this, with larger gains on complex datasets such as CIFAR-100 and Tiny ImageNet compared to CIFAR-10, where baseline accuracy was already high. (ii) Extremely small batch sizes: Relational graphs rely on sufficient pairwise relationships. Very small batches provide limited data context, reducing graph stability and weakening regularization.

I.2 Applicability to Unsupervised and Self-Supervised Learning

Our current GCR formulation relies on ground-truth labels for intra-class masking of the prediction graph. This design was intentional to first establish and validate GCR’s core effectiveness in a fully supervised setting, where we demonstrated consistent, significant gains across diverse architectures and datasets.

However, this reliance is not a fundamental limitation of GCR but rather a characteristic of the current implementation. The core mechanism, aligning feature graph geometry with prediction graph semantics, is flexible. The mask \mathbf{M} can be generated without ground-truth labels, enabling extensions to unsupervised or self-supervised learning. Specifically, we propose two potential adaptations: (i) Pseudo-labeling: In semi/self-supervised settings, high-confidence model predictions can generate pseudo-labels to construct \mathbf{M} , masking pairs sharing the same pseudo-label. (ii) Unsupervised clustering: Feature representations can be clustered dynamically (*e.g.*, via k -means), with \mathbf{M} derived from cluster assignments to enforce consistency among similar samples.

While this work focuses on supervised learning to establish GCR’s principle, the framework is modular. Replacing the ground-truth mask with pseudo-labels or clustering-based masks readily extends GCR to unsupervised domains. This important direction highlights GCR’s broader potential and flexibility.

I.3 Future Works

While GCR introduces a novel and effective mechanism for enhancing semantic structure in deep representations, it also presents several limitations that open up promising avenues for future exploration.

First, GCR currently relies on batch-level relational graphs constructed from intermediate features and softmax predictions. This inherently restricts the global context to within-batch relationships, which may limit its effectiveness in settings with small batch sizes or highly imbalanced class distributions. Exploring memory-augmented or streaming graph variants that accumulate semantic structure across batches could improve scalability and robustness.

Second, although the adaptive weighting mechanism allows the model to prioritize layers with high misalignment, it is currently driven solely by Frobenius distance. More expressive structural metrics, such as spectral divergence, Earth Mover’s distance, or alignment of Laplacian eigenvectors, could offer deeper insights into graph discrepancy and guide more fine-grained supervision.

Third, GCR assumes access to ground-truth labels for masking during training, limiting its current formulation to fully supervised learning. Extending GCR to semi-supervised, self-supervised, or weakly

supervised regimes by deriving prediction graphs from confident pseudo-labels or unsupervised clustering remains an exciting direction.

Fourth, while GCR is model-agnostic and does not alter the architecture, it introduces additional computation from graph construction and alignment. Although lightweight and parallelizable, this cost may still pose challenges in latency-sensitive applications. Investigating more efficient or approximate graph alignment schemes could alleviate this concern.

Finally, our method focuses on classification tasks. Adapting GCR to other modalities and tasks, such as segmentation, detection, or multimodal fusion, requires further study. In particular, integrating GCR with token-level or region-level predictions in transformer models may offer novel insights into semantic alignment beyond image classification.

In future work, we aim to address these limitations by developing more scalable graph construction techniques, expanding the framework to broader learning paradigms, and refining the theoretical understanding of structural supervision in deep networks.

J Broader impacts

GCR introduces a lightweight and architecture-agnostic framework for improving semantic consistency in deep learning models. By aligning intermediate features with structured prediction graphs, GCR encourages networks to learn more coherent, interpretable, and generalizable representations. This has the potential to improve model reliability in critical applications such as medical diagnosis, autonomous driving, and scientific data analysis, where semantic structure and interpretability are crucial.

From an ethical standpoint, GCR does not introduce any explicit biases beyond those already present in the training data. However, like all supervision-driven methods, its effectiveness depends on the quality of labels. If training data contains spurious correlations or mislabeled examples, the alignment process may reinforce rather than correct those artifacts. Future work should investigate ways to make GCR more robust to noisy or biased supervision signals.

GCR is computationally efficient and compatible with existing training protocols, which facilitates deployment in low-resource settings or on edge devices. However, care should be taken to assess environmental costs when scaling to very large models or datasets. In addition, the reliance on pairwise relationships may raise privacy concerns in sensitive domains where sample-wise relationships reveal protected attributes. Applying GCR to privacy-preserving or federated learning settings is a promising direction for ensuring responsible AI development.